Hemodynamics regulate spatiotemporal artery muscularization in the developing circle of Willis

Siyuan Cheng[1,2,3#], Ivan Fan Xia[1,2,3#], Renate Wanner[1,2,3], Javier Abello[4], Amber N. Stratman[4], and Stefania Nicoli[1,2,3*]

[1]Department of Genetics, Yale School of Medicine, 333 Cedar St, New Haven, CT 06520, USA

[2]Yale Cardiovascular Research Center, Section of Cardiology, Department of Internal Medicine, Yale School of Medicine, 300 George St, New Haven, CT 06511, USA

[3]Vascular Biology & Therapeutics Program, Yale School of Medicine, 10 Amistad St, New Haven, CT 06520, USA

[4]Department of Cell Biology & Physiology, School of Medicine, Washington University in St. Louis, 660 S. Euclid Ave, St. Louis, MO 63110, USA

[#] These authors contributed equally

[*] Correspondence to: stefania.nicoli@yale.edu

Abstract

Brain arteries are wrapped by vascular smooth muscle cells (VSMCs). Fully differentiated VSMCs are important for brain artery homeostasis, and they are lost in several cerebrovascular diseases. How healthy VSMCs differentiate on different brain arteries during development is unclear. Such knowledge will help regenerate lost VSMCs in brain arteriopathy. To answer this question, we studied the developmental muscularization of the zebrafish circle of Willis (CW) arteries, the major arterial loop that supplies blood to the brain in all vertebrates. We found that artery specification of CW endothelial cells (ECs) happens after they migrate from primitive veins to form CW arteries. VSMCs differentiate from *pdgfrb*+ common vascular mural cell progenitors at the time when embryo circulation starts and progress temporally and spatially from anterior to posterior CW arteries. Computational fluid dynamic simulation confirms that earlier VSMC differentiation coincide with higher pulsatile flow hemodynamics in anterior CW arteries. Pulsatile blood flow induces the differentiation of human brain *pdgfrb*+ progenitors into VSMCs and reducing pulsatile blood flow by blocking the zebrafish embryo heartbeat after *pdgfrb*+ recruitment but before VSMC differentiation

limits the number of mature VSMCs. Congruently, the flow responsive transcription factor *klf2a* is activated in ECs before VSMC differentiation and knockdown delays VSMC differentiation on CW arteries. Overall, our data place hemodynamic activation of endothelial *klf2a* signaling as key determinant of spatiotemporal VSMC differentiation on CW arteries.

Introduction

Vascular smooth muscle cells (VSMCs) are contractile mural cells wrapping around endothelial cells (ECs) of large vessels, especially arteries (Ando et al., 2022; Donadon & Santoro, 2021; Stratman et al., 2020). The expression of contractile proteins, such as alpha-smooth muscle actin (encoded by *acta2*), distinguishes VSMC from pericytes, the other type of mural cells primarily associated with small vessels including capillaries (Bahrami & Childs, 2020; Donadon & Santoro, 2021; Stratman et al., 2020). VSMCs are important for arterial homeostasis (Basatemur, Jorgensen, Clarke, Bennett, & Mallat, 2019). In the brain, VSMC constriction and relaxation is essential for functional hyperemia in neurovascular coupling (Hill et al., 2015; Kaplan, Chow, & Gu, 2020). Phenotype switching or dedifferentiation of VSMCs, marked by lower expression of contractile proteins, is prominent in pathological progression of atherosclerosis (Basatemur et al., 2019). Recently, similar VSMC phenotype switching or dedifferentiation have also been described in cell, animal, and human studies of children and adult neurological and cerebrovascular conditions (Aguilar-Pineda et al., 2021; Chou et al., 2022; Milewicz et al., 2010; Oka et al., 2020). These studies suggested that understanding the development of VSMC differentiation on brain arteries might help restore normal VSMC contractility to alleviate various cerebrovascular diseases; such a regenerative strategy requires a deep understanding of how VSMCs acquire a contractile phenotype while differentiating from their progenitors.

VSMCs spatially differentiate from different progenitors from mesoderm and neural crest origin (Ando et al., 2019; Donadon & Santoro, 2021; Whitesell et al., 2019). Previous research described various mechanisms regulating the differentiation of VSMC positive for *acta2* in the trunk vasculature. Arterial Notch signaling activated by blood

flow is necessary for *acta2*+ VSMC appearance on the zebrafish dorsal aorta (X. Chen, Gays, Milia, & Santoro, 2017). Autonomous Notch activation is required for specification of *pdgfrb*+ mural cell progenitors from mesenchyme around arteries, and these progenitors later differentiate into *acta2*+ VSMCs (Ando et al., 2019). Chemokine signaling promotes VSMCs association with the zebrafish dorsal aorta in the trunk, whereas blood flow modulated transcription factor krüppel-like factor 2 (encoded by *klf2a* in zebrafish) prevents their association with the adjacent cardinal vein (Stratman et al., 2020). Differentiation into *acta2*+ VSMCs from *pdgfrb*+ progenitors in the brain requires autonomous expression of an ATP-sensitive potassium channel (Ando et al., 2022). In contrast, *acta2*+ VSMCs in the ventral head of zebrafish are not derived from *pdgfrb*+ progenitors, and their differentiation is regulated by endothelial BMP signaling (Watterston, Zeng, Onabadejo, & Childs, 2019; Whitesell et al., 2019). These studies suggested that VSMC differentiation is highly organotypic and may even be vessel specific.

The circle of Willis (CW) consists of major arteries that supply blood to the vertebrate brain, including the internal carotid arteries and posterior communicating arteries (Campbell et al., 2019; Schröder, Moser, & Huggenberger, 2020). CW arteries are wrapped by VSMCs, and VSMC dedifferentiation and hyperplasia are described in carotid atherosclerosis and the pediatric Moyamoya disease (Chou et al., 2022; Fox, Dorschel, Lawton, & Wanebo, 2021). The internal carotid arteries in the CW are among the earliest circulated arteries in the brain due to their connection to the common carotid arteries (lateral dorsal aorta in zebrafish) (Campbell et al., 2019; Isogai, Horiguchi, & Weinstein, 2001; Schröder et al., 2020). VSMC differentiation on CW arteries, particularly internal carotid arteries, and whether this differentiation is associated with early arterial blood flow in the brain, have not been investigated. The mouse CW resembles that of humans, but its VSMC differentiation is difficult to observe *in vivo*, as the embryos develop in utero and depend on maternal circulation (Isogai et al., 2001; Schröder et al., 2020). The zebrafish CW also resembles that of humans, and the embryos external growth and optical clarity allows for confocal live imaging of developing blood vessels (Isogai et al., 2001). In addition, a few fluorescent transgenic (Tg) lines have been generated to label VSMCs and their progenitors (Ando et al., 2016;

Whitesell et al., 2014). Taking advantage of the zebrafish model, we found a spatiotemporal pattern of VSMC differentiation on CW arteries, and we associated this pattern with hemodynamic signaling pathways in arterial ECs.

CW vessel nomenclature	
CaDI	Caudal division of the internal carotid artery
BCA	Basal communicating artery
PCS	Posterior communicating segment

Results

Artery muscularization is spatiotemporally regulated in the CW arteries

Arterial ECs in zebrafish brain emerge from primitive veins (Fujita et al., 2011). Recent single-cell transcriptome profiling of vascular cells in prenatal human brain also supported the fate progression from venous to arterial ECs (Crouch et al., 2022). To establish the stage of CW artery specification in the zebrafish brain, we performed confocal live imaging of Tg(*flt4:yfp*)^{hu4881}, which labels venous ECs, and Tg(*kdrl:hras-mcherry*)^{s896}, which labels all ECs, at four stages starting at 32 hour post-fertilization (hpf), when CW arteries are assembling (Chi et al., 2008; Hogan et al., 2009; Isogai et al., 2001). As arterial ECs express higher *kdrl*, we used the intensity of *mcherry* as an indicator of artery specification (Figure 1A-1E) (Chi et al., 2008). We found that ECs in CW arteries are primarily venous at 32 hpf (Figure 1A and 1E), and gradually gain *kdrl* expression from 54 hpf to 3-day post fertilization (dpf) (Figure 1B, 1C, and 1E). The *mcherry* intensity at 4 dpf is similar to 3 dpf, suggesting that artery specification of the CW is completed by 3 dpf (Figure 1C-1E).

Then we characterized CW artery muscularization. Previous research on the CW arteries described that VSMCs derive from *pdgfrb*+ mural cell progenitors (Ando et al., 2022; Ando et al., 2019). Thus, to determine VSMC differentiation in real time we

performed confocal live imaging of Tg(*acta2:mcherry*)^{ca8}, TgBAC(*pdgfrb:egfp*)^{ncv22}, and Tg(*kdrl:cerulean*)^{sd24}, to visualize respectively VSMCs (red), *pdgfrb*+ progenitors (green) and the developing arteries (white) at four stages starting from 32 hpf (Ando et al., 2016; Page et al., 2013; Whitesell et al., 2014). We found that overall *pdgfrb*+ progenitors appear on CW arteries after their lumen form around 54 hpf, and most of them do not express *acta2* (Figure 2A-2B, 2E-2F, and S1A-S1B). The number of *pdgfrb*+ progenitors increase temporally from 54 hpf to 3 dpf and spatially on CW arteries from anterior to posterior - from the internal carotid arteries (CaDI), the basal communicating artery (BCA) to the posterior communicating segments (PCS) (Figure 2B-2C). Notably, while many *pdgfrb*+ progenitors on CaDI differentiate into *acta2*+ VSMCs by 3 dpf nearly no *acta2*+ VSMCs were observed in the nearby artery BCA or PCS (Figure 2B-2C, 2E-2F, and S1A-S1B). By 4 dpf, the number of *pdgfrb*+ cells is similar to 3 dpf, but *acta2*+ VSMCs on CaDI continue to differentiate in a greater number over the BCA, and PCS arteries (Figure 2C-2F and S1A-S1B). These results show an anterior to posterior differentiation of *pdgfrb*+ progenitors into *acta2*+ VSMCs with the CaDI being the first CW artery muscularized and having a higher number of *acta2*+ VSMCs.

CW arteries have spatiotemporal difference in hemodynamics

Our data suggest that VSMCs in the anterior CaDI differentiate significantly earlier than the anterior BCA and the posterior PCS, even if their progenitors have the same origin and these CW blood vessel formation and arterialization occurs at the same time. We speculate that different hemodynamic distribution may contribute to the spatiotemporal difference in VSMC differentiation on CW arteries. In fact, CaDI is the only vessels in the CW receiving pulsatile arterial blood flow directly from the lateral dorsal aorta and cardiac outflow tract. Furthermore, the CaDI differs from the BCA or PCS in terms of overall vascular geometry, which has been shown to affect local intravascular forces such as the wall shear stress (WSS) (Katritsis et al., 2007). To explore this possibility, we performed microangiography with a high molecular weight fluorescent dextran and used computational fluid dynamics (CFD) to simulate the effect

of pulsatile flow on the CW intravascular forces (ANSYS, 2014; Z. Chen et al., 2019; Fernandes et al., 2022). First, we determined each CW artery diameter, the principal determinant of hemodynamics, and found that there was no significant difference between structures (Figure 3A-3D). Notably, however, the flow velocity across CW arteries was differentially distributed, with the CaDI having the highest blood flow speed starting from 54 hpf to 4 dpf (Figure 3A-3C, and 3E). This is consistent with the CaDI being the inlet vessel for the arterial blood flow within the entire CW circulation. Next, we calculated the WSS across all CW arteries and found an overall increase in average and total WSS from 54 hpf to 4 dpf (Figure 3A-3C, and 3F). Importantly, however, when analyzed individual vessels, we found that the WSS in the CaDI is significantly higher from 54 hpf to 4 dpf, while this increase was not noted in the BCA or PCS (Figure 3A-C, and 3G). Further, WSS in the CaDI is significantly higher than in the BCA and PCS at 3 dpf (Figure 3G), when considerable VSMC differentiation starts on the CaDI but not the BCA or PCS (Figure 2B-2C, 2F, and S1A-S1B). Altogether, the pulsatile blood flow simulation suggests that CW arteries experience different hemodynamic loads that might confer an heterogenous muscularization of CW arteries.

Blood flow is required for differential CW artery muscularization

Our data suggest that ECs under pulsatile arterial flow might favor the differentiation of *acta2*+ VSMCs from *pdgfrb*+ progenitors. To test this hypothesis, we set up an *in vitro* cell co-culture experiment where GFP-PDGFRB+ human brain pericytes (GFP-HBVPs) were cultured in flow amenable outlet slides, then covered by a thin layer of collagen type 1. Confluent human endothelial cells (HUVECs) were seeded on top of that and then exposed to steady-state laminar flow or pulsatile flow conditions (Figure 4A) (Abello, Raghavan, Yien, & Stratman, 2022). Maturation of PDGFRB+ human brain pericytes into ACTA2+ VSMCs was then quantified after 24 hours from the introduction of flow addition. We found that brain pericytes under pulsatile flow were larger and showed higher expression of VSMC differentiation markers including PDGFRB, ACTA2, and TRANSGELIN (Robin et al., 2013) (Figure 4B-4D), suggesting that pulsatile blood flow favored PDGFRB+ progenitor differentiation.

Next, we tested the effect of pulsatile flow in the CW on VSMC differentiation *in vivo*. Previous research suggested that blood flow hemodynamics is not necessary for *pdgfrb*+ progenitor recruitment at CW arteries, as shown by zebrafish embryos lacking blood flow such as the *tnnt2a* morphants (MO) (Ando et al., 2016), however their differentiation to *acta2*+ cells has not been documented. Thus, to determine whether blood flow affects *acta2*+ VSMC differentiation on CW arteries, we injected 0.35 ng of *tnnt2a* MO into Tg(*acta2:mcherry*, *kdrl:gfp*)$^{ca8/zn1}$ at the one to two-cell stage, to abrogate cardiac contractility and thus pulsatile flow (Sehnert et al., 2002; Whitesell et al., 2014; Zhong et al., 2006). Notably, we found no *acta2*+ VSMCs on CW arteries of *tnnt2a* MO at 3 to 4 dpf (Figure 4F, 4H-4I, and 4K), suggesting that blood flow is dispensable for *pdgfrb*+ progenitor recruitment but is required for *acta2*+ VSMC differentiation on the CW arteries.

To further explore the temporal requirement of blood flow, we treated embryos with 25 μM nifedipine, a drug shown to reduce heart rate in zebrafish embryos (Gierten et al., 2020), from 54 hpf, right before the onset of *pdgfrb*+ progenitors' expression of *acta2* (Figure. 2A and B). We found that after 18 hours at 3 dpf the number of *acta2*+ VSMCs is greatly reduced on the CaDI of treated embryos compared to untreated controls (Figure 4G and 4M); *acta2*+ VSMCs on the BCA and the PCS at 4 dpf are also reduced significantly (Figure 4L and 4N), suggesting that blood flow reduction after 54 hpf delays VSMC differentiation on CW arteries with the earliest and strongest effect on the CaDI muscularization (Figure 4G and 4M).

To determine whether blood flow is differentially required for the maintenance of VSMCs on CW arteries, we treated embryos with nifedipine from 4 dpf, after VSMC differentiation on CW arteries, and imaged at 5 dpf. The number of *acta2*+ VSMCs on the CaDI and PCS in treated embryos is similar to untreated controls (Figure S2A-S2C), suggesting that blood flow is required for differentiation but not for short-term maintenance of VSMCs.

Blood flow-regulated transcription factor klf2a is required for spatiotemporal CW artery muscularization

Our results suggest that ECs might express a flow pattern-dependent transcriptional program that favors spatiotemporal VSMC muscularization in the CW arteries. For example, previous studies showed that the site and level of the transcription factor *Klf2* (Parmar et al., 2006; Sweet, Fan, Hsieh, & Jain, 2018; Warboys, Amini, de Luca, & Evans, 2011) in artery ECs closely follow the predicted pattern of elevated intravascular forces (Lee et al., 2006). Consistently, higher *Klf2* expression can be induced by unidirectional pulsatile flow mimicking arterial flow (Dekker et al., 2002). Furthermore, *klf2* is implicated in VSMC migration on arterial blood vessels during mouse development: loss of *klf2* leads to aorta VSMC deficiency (Wu, Bohanan, Neumann, & Lingrel, 2008) while endothelial *klf2a* expression prevents VSMC association with primitive veins in zebrafish trunk (Stratman et al., 2020). Hence, we tested the hypothesis that *klf2a* might be the signaling spatially regulated in the CW artery to control VSMC maturation. We first imaged Tg(*klf2a:h2b-egfp*, *kdrl:hras-mcherry*)$^{ig11/s896}$, which labels nuclei with active *klf2a* expression, and quantified the number of *klf2a*+ ECs in the CW arteries (Chi et al., 2008; Steed et al., 2016). To account for the overall changes in EC number during development (Ulrich, Ma, Baker, & Torres-Vazquez, 2011), as well as the length of each vessels, we also imaged Tg(*fli1:nls-gfp*, *kdrl:hras-mcherry*)$^{y7/s896}$, which labels all EC nuclei, at four stages from 32 hpf (Roman et al., 2002). Notably, we found a slight increase in ECs number per 100 μm vessel in the CaDI from 32 to 54 hpf (Figure S3A-S3C), but a much more significant increase in *klf2a*+ EC nuclei in the CaDI (Figure 5A and 5B), before *acta2*+ VSMCs appear (Figure 2B-2C, 2F, and Figure S1A-S1C). The number of ECs in the CaDI stayed the same from 54 hpf through 4 dpf (Figure S3A-S3C), while *klf2a*+ ECs in the CaDI increased until 3 dpf (Figure 5A and 5B). In tandem, *acta2*+ VSMCs on the CaDI increase through 4 dpf (Figure 2C-2D, 2F, and Figure S1A-S1C). EC number per 100 μm vessel in the BCA and PCS are similar from 54 hpf to 4 dpf (Figure S3A-S3C), whereas the number of *klf2a*+ ECs increase significantly over time (Figure 5A and 5B). This increase predates the presence of *acta2*+ VSMCs on the BCA and PCS (Figure 2B-2D, 2F, and Figure S1A-S1C). These results suggest that the increase of *klf2a*+ ECs in the CW arteries is not due to an increase in EC number and precedes the spatiotemporal VSMC differentiation observed on the CW arteries.

To further define the role of *klf2a* in CW artery muscularization, we knocked down *klf2a* in Tg(*acta2:mcherry*, *kdrl:gfp*)$^{ca8/zn1}$ with 11 ng MO injection at the one to two-cell stage and imaged at 3 to 4 dpf (Nicoli et al., 2010; Whitesell et al., 2014; Zhong et al., 2006). We validated the effect of *klf2a* MO knockdown using the Tg(*klf2a:h2b-egfp*, *kdrl:hras-mcherry*)$^{ig11/s896}$ transgenic line (Figure S3D-S3F) (Chi et al., 2008; Steed et al., 2016). Compared to uninjected control, *klf2a* morphants have significantly less *acta2*+ VSMCs on the CaDI at 3 dpf but a normal number by 4 dpf (Figure 6A-6D), suggesting that *klf2a* promotes timely initiation of CaDI muscularization. Together these data suggest that CW muscularization is associated with endothelial *klf2a* activation and necessary for spatiotemporal VSMC differentiation under pulsatile blood flow conditions.

Discussion

Here, we used confocal live imaging of fluorescence transgenic zebrafish embryos to characterize the spatiotemporal dynamics of VSMC differentiation on the CW, which consists of major arteries that supply blood to the vertebrate brain. We found that CW morphogenesis preceded arterial specification. *pdgfrb*+ mural cell progenitors start to express the VSMC marker *acta2* after these mural cell progenitors were recruited to CW arteries. VSMCs differentiated earlier on anterior CW arteries, which are under higher WSS than their posterior counterparts, due to the high velocity of incoming pulsatile blood flow. We used an *in vitro* co-culture assay, genetic manipulation, and drug treatments to provide evidence that pulsatile blood flow can contribute to spatiotemporal VSMC differentiation. We found that the flow responsive transcription factor *klf2a* is activated from anterior to posterior in the CW arteries, preceding VSMC differentiation. *klf2a* knockdown delayed VSMC differentiation on anterior CW arteries. Together, these data support the conclusion that pulsatile flow activation of endothelial *klf2a* promotes spatiotemporal VSMC differentiation on CW arteries in the brain (Figure 7).

Our work suggests *klf2a*-mediated blood flow regulation of VSMC differentiation on zebrafish brain arteries, and thus raises the question of how Klf2 transduces endothelial signals to mural cell progenitors and VSMCs. *In vitro*, endothelial Klf2 upregulates miR-143/145, which are transported into co-cultured VSMCs within extracellular vesicles

(EV) to promote a contractile phenotype in VSMCs (Hergenreider et al., 2012). How EV transport of miR-143/145 works *in vivo* during development remains unknown.

Notch signaling appears a plausible downstream effector of Klf2 activation. Like Klf2, Notch also responds to flow in heart valve development (Fontana et al., 2020), and Klf2 appears to upregulate Notch (Duchemin, Vignes, & Vermot, 2019). Non-canonical Notch signaling is induced by shear stress to mediate endothelial barrier formation (Polacheck et al., 2017). Notch1 is a proposed mechanosensor in adult arteries (J. J. Mack et al., 2017). In addition, Notch regulation of VSMC development is well established. Additionally, flow activation of Notch in the dorsal aorta (DA) is required for VSMC recruitment (X. Chen et al., 2017). Notch signaling is also activated in DA VSMC progenitors during development, when DA ECs express Jag1 (jagged canonical Notch ligand 1) (Chang et al., 2012; High et al., 2008). Notch2 and Notch3 are compensatory for VSMC development on the DA (Q. Wang, Zhao, Kennard, & Lilly, 2012). In VSMC differentiation on coronary arteries, ECs express Jag1 and pericyte progenitors express Notch3 (Volz et al., 2015). Thus, reciprocal Notch signaling between ECs and VSMCs may regulate VSMC differentiation on brain arteries, although how Notch signaling activates Myocd (myocardin) (Huang et al., 2008; Li, Wang, Wang, Richardson, & Olson, 2003), Srf (serum response factor) (C. P. Mack & Owens, 1999), and miR-143/145 (Boettger et al., 2009) to enable expression of Acta2 and other contractile proteins remain incompletely understood.

It is important to recognize the versatile roles of Notch signaling in vascular development for process both prior to and in tandem with VSMC differentiation. Notch signaling represses proliferation of arterial ECs during angiogenesis (Hasan et al., 2017; Pitulescu et al., 2017), and maintains arterial identity after morphogenesis (Lawson et al., 2001; Shutter et al., 2000; Villa et al., 2001). Notch signaling is required for recruitment of mural cells to brain arteries, in which Notch2 and Notch3 are redundant for upregulation of Pdgfrb in mesenchymal progenitors (Ando et al., 2019). Notch3, in which mutations cause cerebral autosomal dominant arteriopathy with subcortical infarcts and leukoencephalopathy (CADASIL), is broadly required for mural cell development in the brain (Domenga et al., 2004; Joutel et al., 1996; Y. Wang, Pan,

Moens, & Appel, 2014). Thus, thorough dissection of how Notch signaling regulates VSMC differentiation on brain arteries would require development of novel methods that enable spatiotemporal resolution of Notch ligands and receptors in different vascular cell types.

Wnt signaling is another possible downstream effector of Klf2. In heart valve development, endocardial Klf2 upregulates Wnt9 (wingless-type MMTV integration type family member 9), which activates Wnt signaling in neighboring mesenchymal cells and thereby regulates their proliferation and condensation (Goddard et al., 2017). The pathway interacts with Notch signaling in heart valve morphogenesis (Paolini, Fontana, Pham, Rodel, & Abdelilah-Seyfried, 2021). Non-canonical Wnt signaling attenuates EC sensitivity to shear stress and stabilizes blood vessels (Franco et al., 2016). In brain vascular development, Wnt signaling controls brain specific developmental angiogenesis and endothelial barrier formation (Daneman et al., 2009; Liebner et al., 2008; Zhou et al., 2014). Wnt signaling in mural cells activates expression of Lama2 (laminin subunit alpha 2), a major component of the brain vascular basement membrane, to promote the neurovascular unit and blood-brain barrier maturation (Biswas et al., 2022). Wnt signaling regulates VSMC proliferation, migration, and survival in cardiovascular diseases (Mill & George, 2012), but relatively little is known about the role of Wnt signaling in VSMC differentiation, especially organotypic VSMC differentiation on brain arteries.

The biochemical pathway by which Klf2 activates Notch or Wnt signaling remains incompletely understood. Recent chromatin occupancy and transcription studies showed that Klf2 has context specific binding patterns and transcriptional targets in the heart and lung endothelium (Sweet et al., 2023). Thus, Klf2 may have multiple direct or indirect paths to activate Notch or Wnt signaling. The context specificity may also explain different effects of *klf2a* on VSMC development in the zebrafish brain and trunk: previous research suggested that *klf2a* expression in the cardinal vein prevents VSMC association (Stratman et al., 2020), whereas this study suggests that *klf2a* activation in brain arteries promotes VSMC differentiation. It is plausible that *klf2a* has different

expression levels, binding patterns, transcriptional targets, and downstream effects in brain arterial ECs compared with trunk venous ECs.

Our findings raise interesting new questions on whether stable *klf2a* expression in CW arterial ECs supports further maturation of VSMCs. Previous research found that *acta2*+ VSMCs on the BCA and PCS express pericyte enriched *abcc9* (ATP binding cassette subfamily C member 9) at 4 dpf (Ando et al., 2022), which is gradually lost from 5 dpf to 6 dpf (Ando et al., 2022) as these cells become *acta2*+. Interestingly, *acta2*+ VSMCs on CaDI, BCA, and PCS still retain expression of *pdgfrb* at 6 dpf (Ando et al., 2021). Thus, it is possible that stable expression of *klf2a* in CW arterial ECs will support later on complete VSMC maturation, for example in Transgelin positive cells (Colijn, Nambara, & Stratman, 2023). Alternatively, *acta2*+ VSMCs with *pdgfrb* expression are maintained as such in the CW arteries (Ando et al., 2021).

It is important to note the differences between the trunk and our data focused on the CW brain arterial VSMC differentiation. On the dorsal aorta of the trunk, as soon as VSMCs are recruited, they begin expressing Acta2 and Tagln, suggesting simultaneous recruitment and differentiation from sclerotome progenitors (Ando et al., 2016; Stratman et al., 2017), compared with the spatiotemporal dynamics we see on brain arteries. It is also important to note the difference between arterial and venous VSMCs. Brain arterial VSMCs strongly express Acta2, whose expression is weak in venous VSMCs (Crouch, Joseph, Marsan, & Huang, 2023; Hill et al., 2015). Venous VSMCs share more common gene expression signature with pericytes, as they both express Abcc9 and Kcnj8 (Ando et al., 2019; Bondjers et al., 2006; Chasseigneaux et al., 2018; He et al., 2016; Vanlandewijck et al., 2018). Based on our data, it is possible to speculate that pulsatile flow reinforces brain arterial specification before VSMC differentiation. Pulsatile flow contributes to both arterial specification and VSMC differentiation, although the two processes are difficult to dissect *in vivo*, as both require Notch signaling and overlap temporally. In addition, pulsations dampen from dorsal aorta to internal carotid arteries, and flow eventually becomes stable in capillaries and veins (Humphrey & Schwartz, 2021). Current *in vivo* methods involving genetic manipulations and drug treatments are only capable of qualitative reduction in all types of flow, including pulsatile. *In vitro* three-

354 dimensional (3D) vascular culture models, which combine ECs and mural cells
355 (Mirabella et al., 2017; Vila Cuenca et al., 2021), could be further optimized to simulate
356 complex geometry of brain arteries. Combining these models with microfluidics, which
357 allows precise calibration of flow velocity and pulse, would enable a more thorough
358 analysis of endothelial mechanotransduction and its contribution to VSMC differentiation
359 on different arterial beds (Abello, Raghavan, Yien, & Stratman, 2022; Gray & Stroka,
360 2017; Griffith et al., 2020).

361 In conclusion, our work highlights organotypic differences in VSMC differentiation in
362 the CW brain arteries and points to hemodynamics as a main driver of spatiotemporal
363 dynamics of VSMC maturation on the brain arteries. Impaired VSMC differentiation in
364 development could be implicated in cerebrovascular diseases, such as Moyamoya
365 disease, which is linked to mutations in the human *ACTA2* gene that results in VSMC
366 hyperplasia specifically on the internal carotid arteries (Fox et al., 2021; Guo et al.,
367 2007; Guo et al., 2009; Lin et al., 2012). Our study points to endothelial cell
368 mechanotransduction of pulsatile flow as a key signaling network that could render
369 specific VSMC populations on brain arteries more susceptible compared to VSMCs
370 associated with other vessels in the same tissue. Our data will therefore inform the
371 screening of new genes that in combination to known genetic variants, such as *ACTA2*,
372 could contribute to our understanding of the susceptibilities in cerebrovascular diseases.

373

374 **Material and Methods**

375 Zebrafish husbandry and transgenic lines

376 Zebrafish were raised and maintained at 28.5 °C using standard methods. Protocols
377 are approved by the Yale Institutional Animal Care and Use Committee (2020-11473).
378 Transgenic lines in Table 1 were established previously.

379 Table 1. List of zebrafish fluorescent transgenic lines used in the study

Transgenic Line	ID	Lab of Origin	Reference

Tg(*flt4:yfp*)^{hu4881}	ZDB-ALT-100208-1	S. Schulte-Merker	Hogan et al., 2009
Tg(*kdrl:hras-mcherry*)^{s896} [Tg(*kdrl:ras-mcherry*)^{s896}]	ZDB-ALT-081212-4	D.Y.R. Stainier	Chi et al., 2008
Tg(*acta2:mcherry*)^{ca8}	ZDB-ALT-120508-2	S.J. Childs	Whitesell et al., 2014
TgBAC(*pdgfrb:egfp*)^{ncv22}	ZDB-ALT-160609-1	N. Mochizuki	Ando et al., 2016
Tg(*kdrl:cerulean*)^{sd24}	ZDB-ALT-131024-2	D. Traver	Page et al., 2013
Tg(*kdrl:grcfp*)^{zn1} [Tg(*kdrl:gfp*)^{zn1}]	ZDB-ALT-051114-10	Zygogen Research Department	Cross et al., 2003
Tg(*klf2a:h2b-egfp*)^{ig11}	ZDB-ALT-161017-10	J. Vermot	Steed et al., 2016
Tg(*fli1:negfp*)^{y7} [Tg(*fli1:nls-gfp*)^{y7}]	ZDB-ALT-060821-4	B.M. Weinstein	Roman et al., 2002

Confocal fluorescence microscopy

Zebrafish embryos were raised in 0.003% 1-phenyl-2-thiourea (PTU, phenylthiocarbamide, or n-phenylthiourea, Sigma P7629) from gastrulation stage to prevent pigmentation. Embryos imaged live by confocal fluorescence microscopy were anesthetized in 0.1% tricaine methanesulfonate (TMS, MS-222, or Syncaine, Western Chemical, NC0872873) and mounted in 1% low melt agarose within glass bottom microwell dishes. Fluorescence images were captured with an upright Zeiss LSM 980 confocal microscope using a 20X objective.

Image analysis

Confocal fluorescence images were analyzed with Imaris microscopy image analysis software (Bitplane, Oxford Instruments). Average fluorescence intensity of mcherry in Tg(*flt4:yfp, kdrl:hras-mcherry*)$^{hu4881/s896}$ was estimated by generating volume objects covering the artery of interest with Surfaces module. Vessel lengths of the arteries were manually traced with Filament module. Numbers of *pdgfrb*+ mural cell progenitors, *acta2*+ vascular smooth muscle cells, and *klf2a*+ and *fli1*+ endothelial nucleus were counted with Spots module.

Morpholino injections

Morpholino antisense oligonucleotides were synthesized by Gene Tools. Morpholinos in Table 2 were validated previously. Optimized dose injected into each embryo are listed. Uninjected siblings were used as controls.

Table 2. List of morpholino antisense oligonucleotides used in the study

Morpholino	Sequence	ID	Reference	Dose (ng/embryo)
MO1-tnnt2a	5' - CATGTTTGCTCTGATCTGACACGCA - 3'	ZDB-MRPHLNO-060317-4	Sehnert et al., 2002	0.35
MO1-klf2a	5' - GGACCTGTCCAGTTCATCCTTCCAC - 3'	ZDB-MRPHLNO-100610-8	Nicoli et al., 2010	11

Nifedipine treatment

Nifedipine was dissolved into 20 mM in dimethyl sulfoxide (DMSO). The stock solution was diluted into 25 μM in egg water with 0.003% PTU to treat zebrafish embryos from 54 hpf to 3 dpf or 4 dpf. The stock solution was diluted into 20 μM in egg water with 0.003% PTU to treat zebrafish embryos from 4 dpf to 5 dpf. The same

409 volume of DMSO was added into egg water with 0.003% PTU for sibling control
410 embryos.

411 Microangiography

412 Embryos were anesthetized in 0.1% tricaine methanesulfonate, placed on an
413 agarose mold, and injected pericardially with 4 nL Tetramethylrhodamine Dextran
414 (2,000,000 molecular weight, Thermo Fisher) at a concentration of 10 mg/mL.
415 Subsequently, the vasculature of embryos was checked for Dextran fluorescence signal
416 under a stereomicroscope (Olympus, MVX10). Embryos with Dextran fluorescence
417 were mounted in 1% low melt agarose within glass bottom microwell dishes and imaged
418 with confocal microscope.

419 Computational fluid dynamic simulation

420 Computational fluid dynamic simulation was performed as previously described with
421 modification (ANSYS, 2014; Barak et al., 2021). Three-dimensional (3D) geometry
422 models of the circle of Willis (CW) arteries were reconstructed from confocal
423 microangiography images of Dextran injected Tg(*kdrl:gfp*) embryos with the Filament
424 module in Imaris (Bitplane, Oxford instruments). The CW 3D geometry models were
425 pre-processed in ANSYS SpaceClaim 2022 R1 software. Pre-processed models were
426 then meshed in ANSYS Fluent 2022 R1 software using computational fluid dynamics
427 application settings. Inlets and outlets were specified. Meshing orthogonal quality was
428 calculated, and objects less than 0.01 were excluded. Blood density and gauge
429 pressure were considered as 1,060 kg/m^3 and 13,332 pascals, respectively. Each
430 analysis consisted of 200 iterations.

431 Cell Culture

432 Pooled primary Human Umbilical Vein Endothelial Cells (HUVEC) (PCS-100-010^{TM},
433 ATCC) were seeded at an initial concertation of 5,000 cells per cm^2, in 1x M119 media
434 (110343-023, Gibco) supplemented with 16% FBS (Gibco), 84 µg/mL of heparin sodium
435 salt (H3393, Sigma-Aldrich), 25 µg/mL of endothelial cell growth supplement (02-102,
436 EMD Millipore Corp.) and 1x Antibiotic-antimycotic solution (15240-062, Gibco). Cell

cultures were maintained at 37^{o}C, 5% CO_2 and 95% humidity, until the cell reached 80% confluence.

To facilitate cell visualization in cell co-cultures, Human Brain Vascular Pericytes (HBVP) (1200, ScienCell) were transfected using lentiviral particles (LVP310, GenTarget, Inc.) to induce GFP expression under EF1a promotor. Cells cultures were initiated by seeding 5,000 cells per cm^2 in 175 cm^2 plastic flasks pre-coated with gelatin and 1x DMEM (11995-065, Gibco) supplemented with 10% FBS (Gibco), and 1x Antibiotic-antimycotic solution under the same cell culture conditions described above. When cells cultures were at 80% confluence, 200 µL containing 2 x 10^6 GFP-lentiviral particles were added to each 175 flasks. After 72 hours, fresh cell culture media supplemented with 10µg/mL of Blasticidin (15205, Sigma-Aldrich) were added to each flask to select the positive transfected cells.

Flow assays and immunostaining

HBVP cells were harvested and seeded at a concentration of 1.3 x 10^5 cells in 0.4 optical plastic flow microslides (80176, Ibidi) precoated with 1 mg/mL gelatin and incubated for 24 hours under standard culture conditions. After the initial incubation, 100 µg/mL of collagen I (354249, Corning) diluted in DMEM cell culture media was added to the slides to create a thin layer on top of the HBVP cells. After 2 hours, the media was removed and 2.5 x 10^5 HUVECs were seeded on top of the collagen I layer and incubated for additional 24 hours. After cell co-cultures were established, the slides were exposed to laminar (15 dyn/cm^2) or pulsatile (12-15 dyn/cm^2) flow for 24 hours, implementing a peristaltic pump adapted to produce different types of flow (Abello, Raghavan, Yien, & Stratman, 2022). After 24 hours, cultures were rinsed with 1x PBS and fixed for 30 minutes in 4% paraformaldehyde at room temperature. Cell cultures were immunostained with α-Smooth muscle actin D4K9N XP® rabbit monoclonal antibody (19245, Cell Signaling), followed by Alexa Fluor 633 goat anti-rabbit IgG (A21071, Invitrogen). Confocal images were obtained using a 40x objective with a W1 Spinning Disk confocal microscope, a Fusion camera, and the Nikon Eclipse Ti2-E base. Fiji image processing software was used for image analysis and fluorescence intensity quantification.

Statistics

All statistical analyses were performed with GraphPad Prism (version 10.0.3). Mann–Whitney test was used to compare two groups to test mean differences (protein level, morpholino and nifedipine treatment). Two-way analyses of variance followed by Tukey's multiple comparisons was used to compare more than two groups to test mean differences (average fluorescence intensity, cell number, vascular diameter, flow velocity, and WSS).

Acknowledgements

We thank the labs of S. Schulte-Merker, D.Y.R. Stainier, S.J. Childs, N. Mochizuki, D. Traver, J. Vermot, and B.M Weinstein for sharing zebrafish transgenic lines. We thank N. Semanchik for all the assistance with zebrafish adult colonies and husbandry. Experiments in the manuscript were supported by R01NS109160 and R01DK118728 awarded to S.N. and AHA23POST1025829 post-doctoral fellowship awarded to I.F.X. The paper is based on a dissertation submitted by S.C. to fulfill in part the requirements for the degree of Doctor of Philosophy, Yale University. S.C. was supported by a Gruber Science Fellowship from Yale Graduate School of Arts and Sciences.

Author Contributions

S.C. and I.F.X contributed to the experiments, the data analysis, and composed the figures. R.W. performed dextran microangiography experiments. J.A. and A.N.S. performed the *in vitro* experiments. S.C., I.F.X and S.N. wrote the manuscript and prepared figures. J.A. and A.N.S. edited the paper.

Figures and Figure Legends

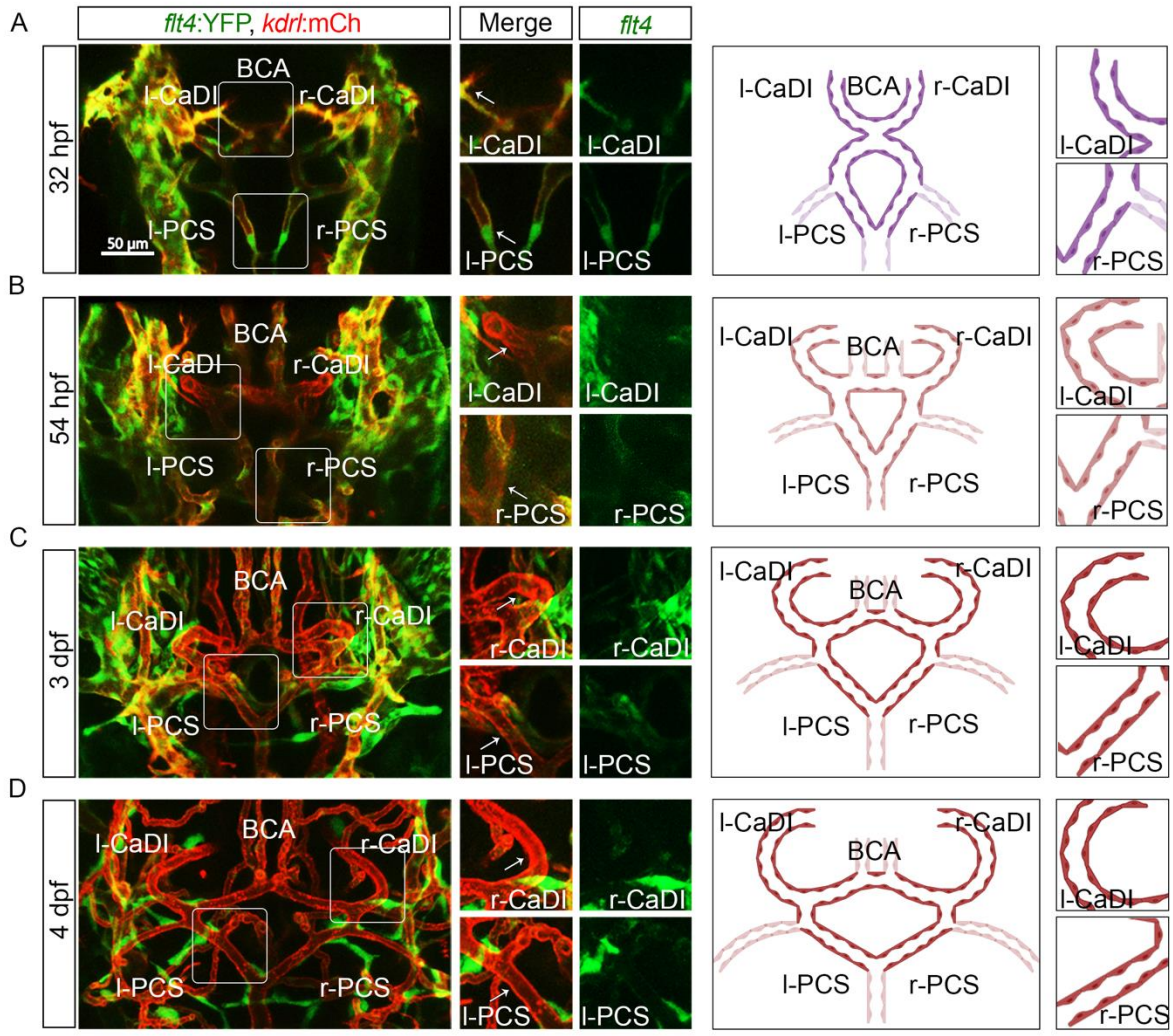

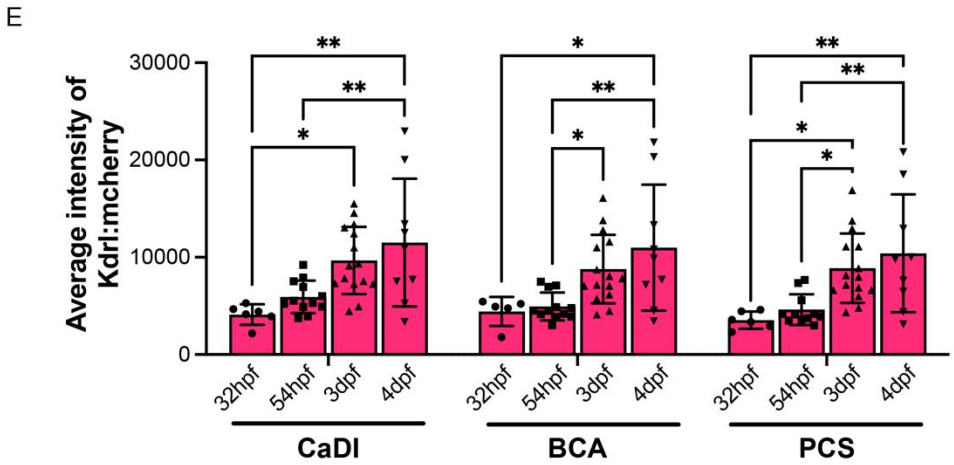

Figure 1. Artery specification of endothelial cells (ECs) in circle of Willis (CW) arteries

(A-D) Confocal live images of Tg(*flt4:yfp*, *kdrl:hras-mcherry*)$^{hu4881/s896}$ and scheme representation of CW arteries in zebrafish brain at 32 hour post fertilization (hpf) (A), 54 hpf (B), 3 day post fertilization (dpf) (C), and 4 dpf (D). Green channel represents *flt4:yfp* fluorescence, Red channel represents *kdrl:hras-mcherry* fluorescence, and Merge panel combines both channels. Arrows point to the CW arteries with *kdrl:hras-mcherry* signal. Scale bar = 50 μm

(E) Average intensity of *kdrl:hras-mcherry* in caudal division of internal carotid arteries (CaDI), basal communicating artery (BCA), and posterior communicating segments (PCS) at 32 hpf (n=6, 2 independent experiments), 54 hpf (n=12, 4 independent experiments), 3 dpf (n=15, 4 independent experiments), and 4 dpf (n=9, 2 independent experiments), two-way analyses of variance followed by Tukey's multiple comparisons, represented with mean ± SD, * $p \leq 0.05$, ** $p \leq 0.01$

Abbreviations: hpf: hour post fertilization, dpf: day post fertilization, EC: endothelial cell, l-CaDI: left caudal division of internal carotid artery, r-CaDI: right caudal division of internal carotid artery, BCA: basal communicating artery, l-PCS: left posterior communicating segment, r-PCS: right posterior communicating segment

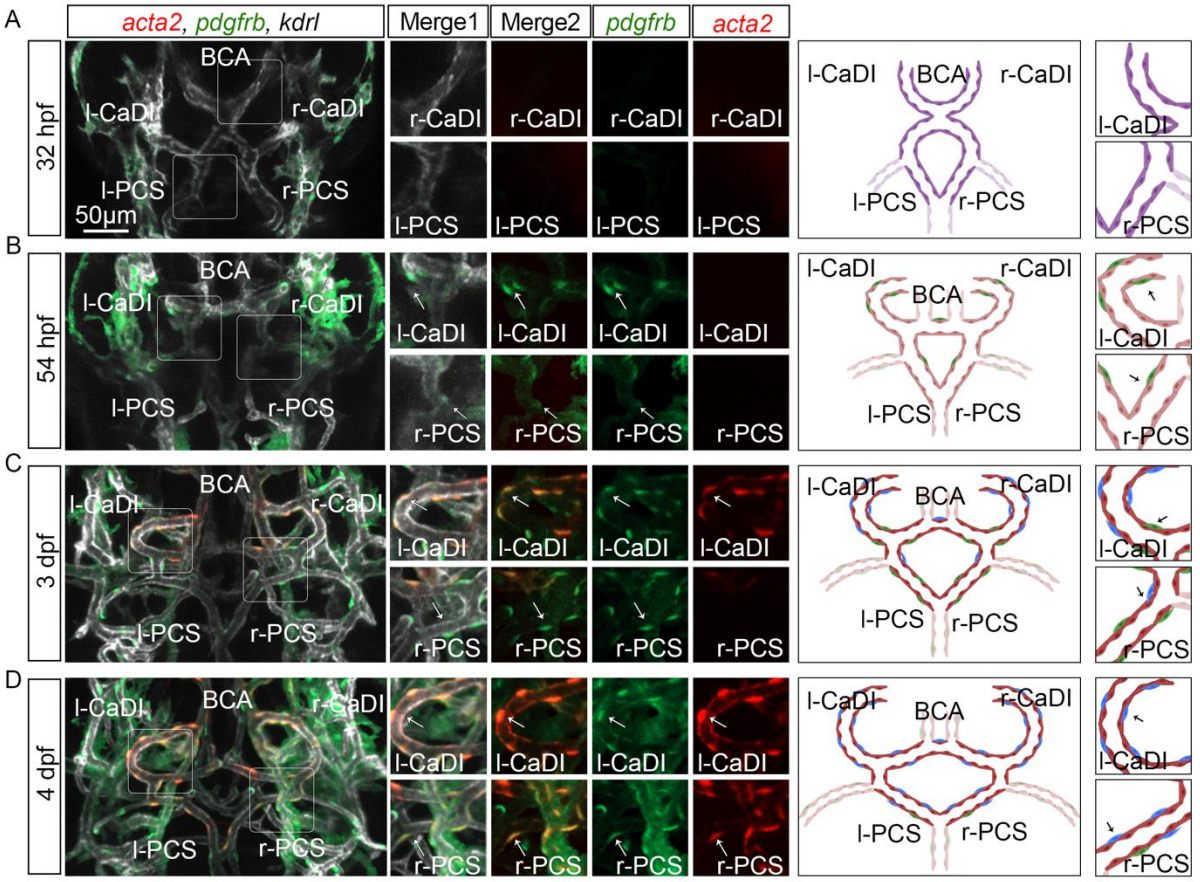

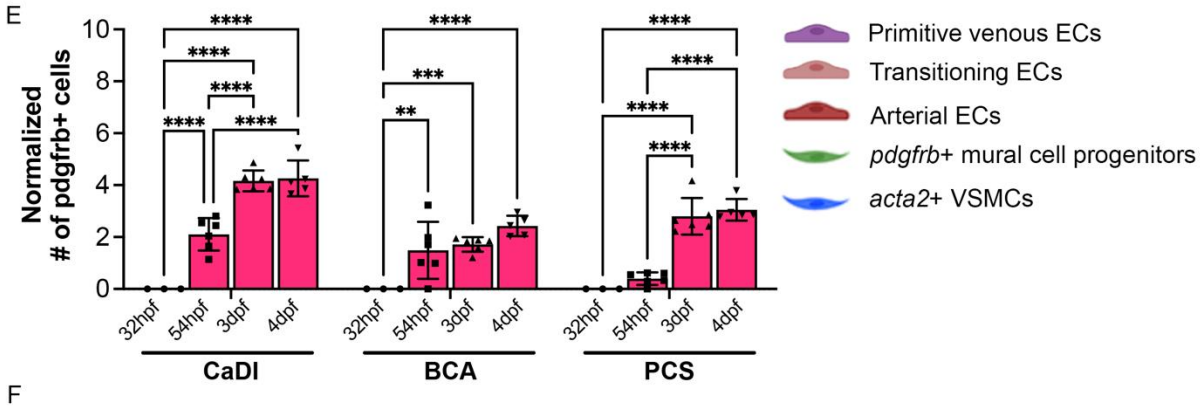

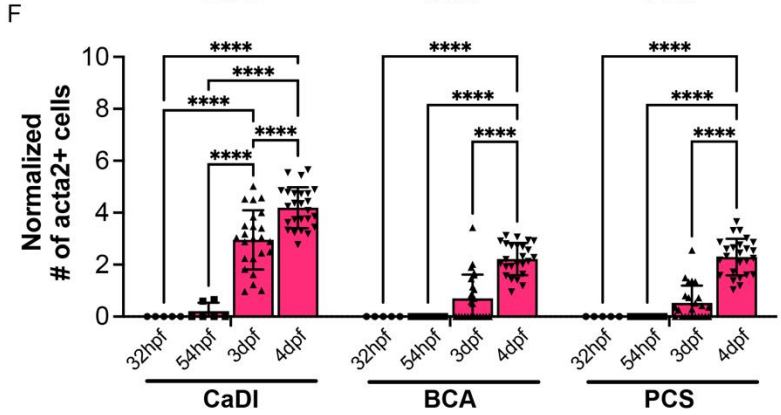

511

Figure 2. Vascular smooth muscle cell (VSMC) differentiation on circle of Willis (CW) arteries

(A-D) Confocal live images of Tg(*acta2:mcherry*, *kdrl:cerulean*)$^{ca8/sd24}$ TgBAC(*pdgfrb:egfp*)^{ncv22} and scheme representation of vascular endothelium and mural cells on CW arteries in zebrafish brain at 32 hour post fertilization (hpf) (A), 54 hpf (B), 3 day post fertilization (dpf) (C), and 4 dpf (D). White channel represents *kdrl:cerulean* fluorescence, Red channel represents *acta2:mcherry*, Green channel represents *pdgfrb:egfp,* Merge 1 panel combines all three channels, Merge 2 combines *acta2:mcherry* in red and *pdgfrb:egfp* in green. Arrows point to the CW arteries with *pdgfrb:egfp* and *acta2:mcherry* signal. Scale bar = 50 μm

(E) Number of *pdgfrb*+ vascular mural cell progenitors per 100 μm vessel length on caudal division of internal carotid arteries (CaDI), basal communicating artery (BCA), and posterior communicating segments (PCS) at 32 hpf (n=3, 1 independent experiment), 54 hpf (n=6, 1 independent experiment), 3 dpf (n=6, 1 independent experiment), and 4 dpf (n=5, 1 independent experiment), two-way analyses of variance followed by Tukey's multiple comparisons, represented with mean ± SD, ** p≤0.01, *** p≤0.001, **** p≤0.0001

(F) Number of *acta2*+ VSMCs per 100 μm vessel length on CaDI, BCA, and PCS at 32 hpf (n=5, 1 independent experiment), 54 hpf (n=6, 2 independent experiments), 3 dpf (n=24, 6 independent experiments), and 4 dpf (n=25, 6 independent experiments), two-way analyses of variance followed by Tukey's multiple comparisons, represented with mean ± SD, **** p≤0.0001

Abbreviations: hpf: hour post fertilization, dpf: day post fertilization, EC: endothelial cell, VSMC: vascular smooth muscle cell, l-CaDI: left caudal division of internal carotid artery, r-CaDI: right caudal division of internal carotid artery, BCA: basal communicating artery, l-PCS: left posterior communicating segment, r-PCS: right posterior communicating segment

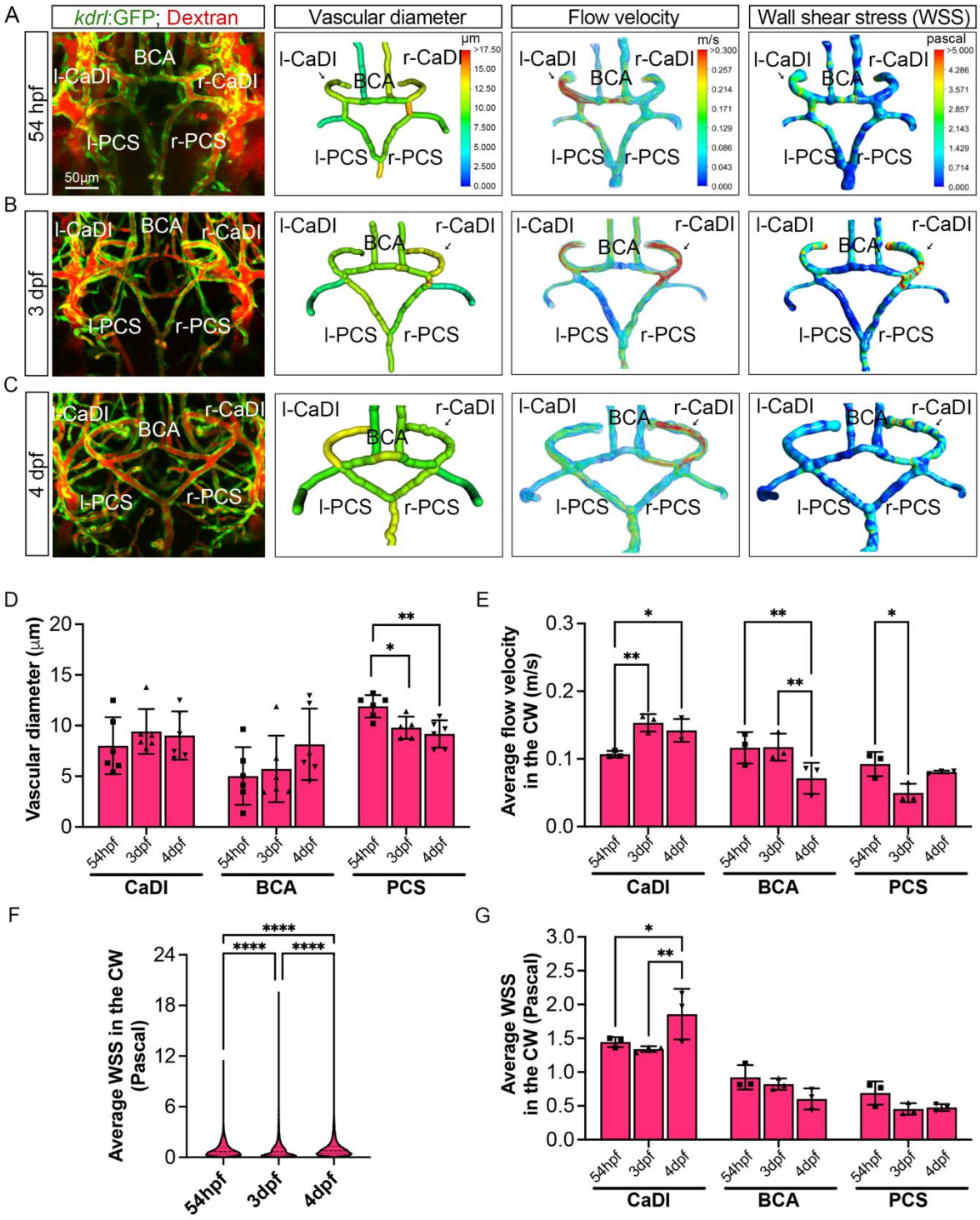

Figure 3. Computational fluid dynamic (CFD) simulation of circle of Willis (CW) arteries

(A-C) Confocal live images of Tg(*kdrl:gfp*)^{zn1} injected with dextran and representation of vascular diameter, CFD simulated wall shear stress (WSS), and flow velocities in CW arteries at 54 hour post fertilization (hpf) (A), 3 day post fertilization (dpf) (B), and 4 dpf (C). Arrows point to the CW arteries with high flow velocity and WSS. Scale bar = 50 μm

(D) Average vascular diameter in caudal division of internal carotid arteries (CaDI), basal communicating artery (BCA), and posterior communicating segments (PCS) at 54 hpf (n=6, 1 independent experiment), 3 dpf (n=6, 1 independent experiment), and 4 dpf (n=6, 1 independent experiment), two-way analyses of variance followed by Tukey's multiple comparisons, * $p \leq 0.05$, ** $p \leq 0.01$

(E) Average flow velocity in CaDI, BCA, and PCS at 54 hpf (n=3, 1 independent experiment), 3 dpf (n=3, 1 independent experiment), and 4 dpf (n=3, 1 independent experiment), two-way analyses of variance followed by Tukey's multiple comparisons, * $p \leq 0.05$, ** $p \leq 0.01$

(F) Average wall shear stress (WSS) throughout the CW arteries at 54 hpf (n=3, 1 independent experiment), 3 dpf (n=3, 1 independent experiment), and 4 dpf (n=3, 1 independent experiment), two-way analyses of variance followed by Tukey's multiple comparisons, **** $p \leq 0.0001$

(G) Average wall shear stress (WSS) in CaDI, BCA, and PCS at 54 hpf (n=3, 1 independent experiment), 3 dpf (n=3, 1 independent experiment), and 4 dpf (n=3, 1 independent experiment), two-way analyses of variance followed by Tukey's multiple comparisons, * $p \leq 0.05$, ** $p \leq 0.01$

Abbreviations: hpf: hour post fertilization, dpf: day post fertilization, WSS; wall shear stress, l-CaDI: left caudal division of internal carotid artery, r-CaDI: right caudal division of internal carotid artery, BCA: basal communicating artery, l-PCS: left posterior communicating segment, r-PCS: right posterior communicating segment

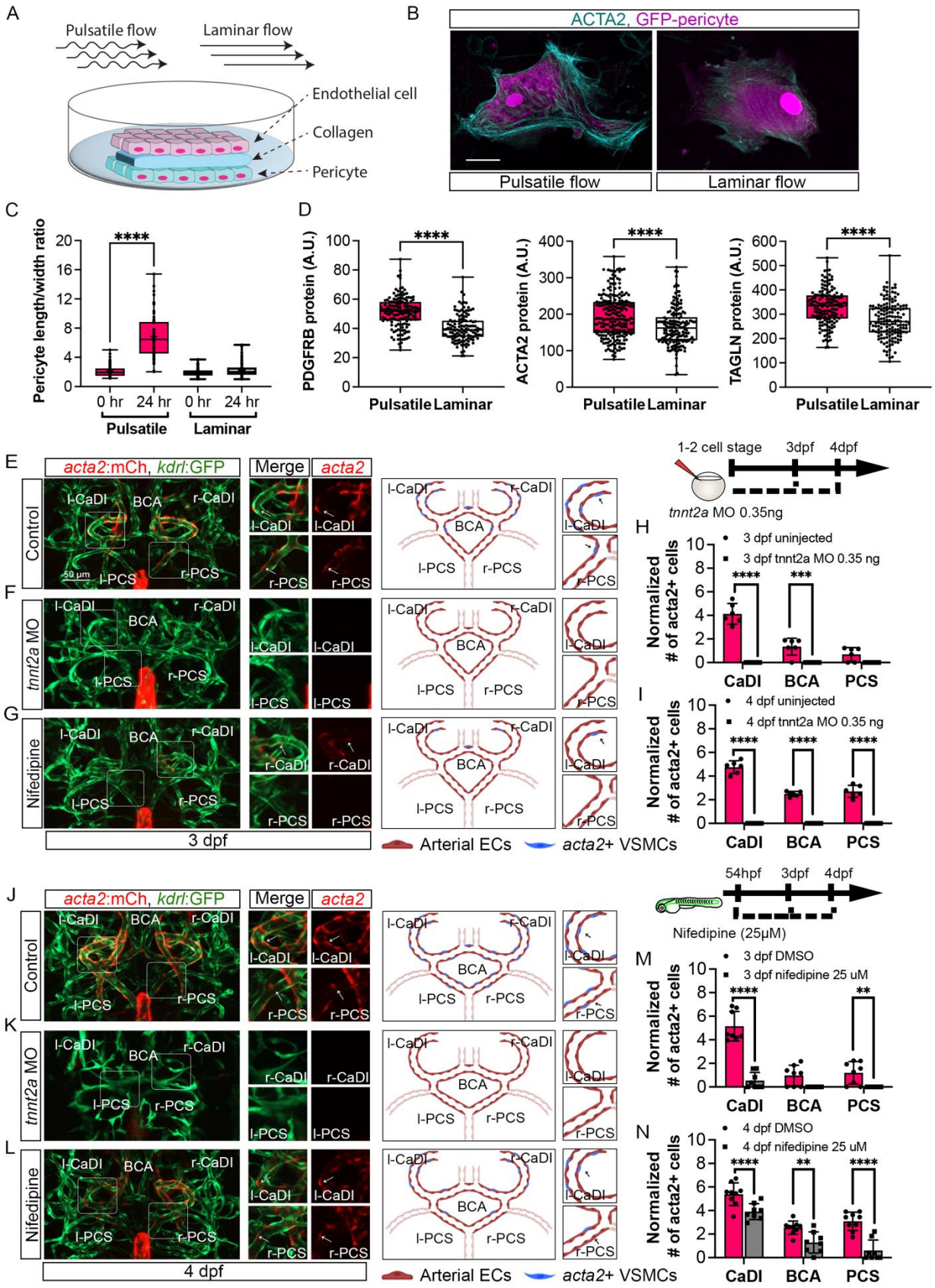

Figure 4. Blood flow is required for vascular smooth muscle cell (VSMC) differentiation on circle of Willis (CW) arteries

(A) Scheme representation of *in vitro* cell co-culture experiment

(B) Representative immunofluorescence images of brain pericytes after exposure of pulsative flow and laminar flow. Cells were stained for ACTA2 (cyan), and cytosolic GFP label (magenta). Scale bar = 10 μm

(C) Morphological measurement of brain pericyte length/width ratio before and after exposure of pulsative flow and laminar flow, 3 independent experiments, two-tailed Mann–Whitney test, represented with mean ± SD, **** p≤0.0001

(D) Protein level of PDGFRB (3 independent experiment), ACTA2 (5 independent experiment), and TAGLN (TRANSGELIN, 3 independent experiment) in arbitrary unit (A.U.) after exposure of pulsative flow and laminar flow, two-tailed Mann–Whitney test, represented with mean ± SD, **** p≤0.0001

(E-G) Confocal live images of Tg(*acta2:mcherry*; *kdrl:gfp*)$^{ca8/zn1}$ and scheme representation of vascular endothelium and VSMCs on CW arteries at 3 day post fertilization (dpf) in control embryos (E), embryos injected with 0.35 ng *tnnt2a* morpholino (MO) (F), embryos treated with 25 μM nifedipine from 54 hour post fertilization (hpf) (G). Red channel represents *acta2:mcherry*, Green channel represents *kdrl:gfp*, and Merge panel combines both channels. Arrows point to the CW arteries with *acta2:mcherry* signal. Scale bar = 50 μm

(H) Number of *acta2*+ VSMCs per 100 μm vessel length on caudal division of internal carotid arteries (CaDI), basal communicating artery (BCA), and posterior communicating segments (PCS) at 3 dpf in uninjected control (n=6, 1 independent experiment) and embryos injected with 0.35 ng *tnnt2a* MO at one to two cell stage (n=6, 1 independent experiment), two-tailed Mann–Whitney test on each vessel's comparison, represented with mean ± SD, *** p≤0.001, **** p≤0.0001

(I) Number of *acta2*+ VSMCs per 100 μm vessel length on CaDI, BCA, and PCS at 4 dpf in uninjected control (n=6, 1 independent experiment) and embryos injected with

595 0.35 ng *tnnt2a* MO at one to two cell stage (n=6, 1 independent experiment), two-tailed
596 Mann–Whitney test on each vessel's comparison, represented with mean ± SD, ****
597 p≤0.0001

598 (J-L) Confocal live images of Tg(*acta2:mcherry*; *kdrl:gfp*)$^{ca8/zn1}$ and scheme
599 representation of vascular endothelium and VSMCs on CW arteries at 4 dpf in control
600 embryos (J), embryos injected with 0.35 ng *tnnt2a* MO (K), embryos treated with 25 µM
601 nifedipine from 54 hpf (L). Red channel represents *acta2:mcherry*, Green channel
602 represents *kdrl:gfp*, and Merge panel combines both channels. Arrows point to the CW
603 arteries with *acta2:mcherry* signal. Scale bar = 50 µm

604 (M) Number of *acta2*+ VSMCs per 100 µm vessel length on CaDI, BCA, and PCS at 3
605 dpf in DMSO control (n=8, 2 independent experiments) and embryos treated with 25 µM
606 nifedipine from 54 hpf (n=8, 2 independent experiments), two-tailed Mann–Whitney test
607 on each vessel's comparison, represented with mean ± SD, ** p≤0.01, **** p≤0.0001

608 (N) Number of *acta2*+ VSMCs per 100 µm vessel length on CaDI, BCA, and PCS at 4
609 dpf in DMSO control (n=9, 2 independent experiments) and embryos treated with 25 µM
610 nifedipine from 54 hpf (n=8, 2 independent experiments), two-tailed Mann–Whitney test
611 on each vessel's comparison, represented with mean ± SD, ** p≤0.01, **** p≤0.0001

612 Abbreviations: hpf: hour post fertilization, dpf: day post fertilization, EC: endothelial cell,
613 VSMC: vascular smooth muscle cell, MO: morpholino, l-CaDI: left caudal division of
614 internal carotid artery, r-CaDI: right caudal division of internal carotid artery, BCA: basal
615 communicating artery, l-PCS: left posterior communicating segment, r-PCS: right
616 posterior communicating segment

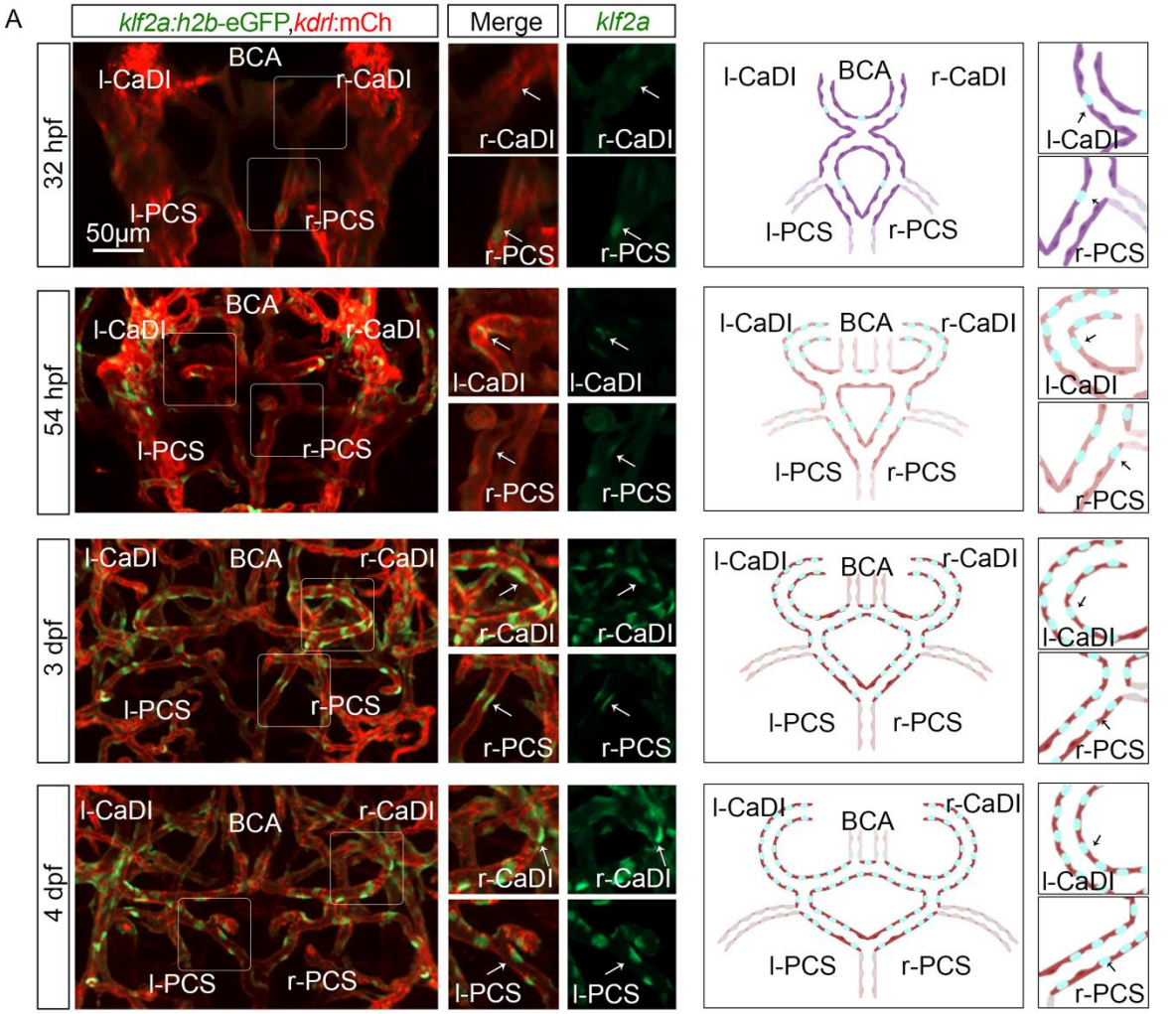

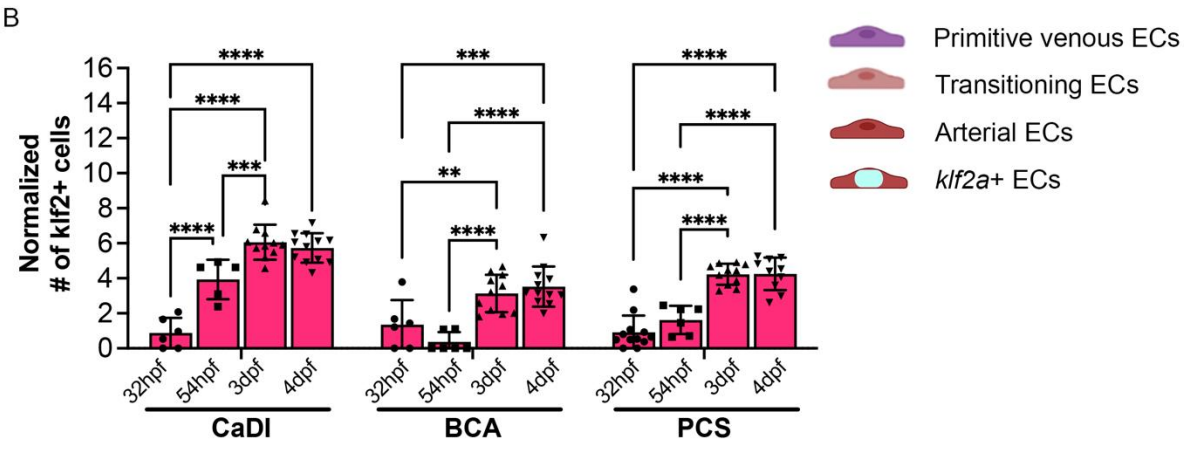

Figure 5. Blood flow regulated transcription factor *klf2a* is expressed in circle of Willis (CW) arteries

(A) Confocal live images of Tg(*klf2a:h2b-gfp*, *kdrl:ras-mcherry*)$^{ig11/s896}$ and scheme representation of endothelial cells (ECs) in CW arteries in zebrafish brain at 32 hour post fertilization (hpf), 54 hpf, 3 day post fertilization (dpf), and 4 dpf. Green channel represents *klf2a:h2b-gfp*, Red channel represents *kdrl:ras-mcherry*, and Merge panel combines both channels. Arrows point to the CW arteries with *klf2a:h2b-gfp* signal. Scale bar = 50 μm

(B) Number of *klf2a*+ ECs per 100 μm vessel length on caudal division of internal carotid arteries (CaDI), basal communicating artery (BCA), and posterior communicating segments (PCS) at 32 hpf (n=6, 3 independent experiments), 54 hpf (n=6, 2 independent experiments), 3 dpf (n=11, 3 independent experiments), and 4 dpf (n=12, 3 independent experiments), two-way analyses of variance followed by Tukey's multiple comparisons, represented with mean ± SD, ** p≤0.01, *** p≤0.001, **** p≤0.0001

Abbreviations: hpf: hour post fertilization, dpf: day post fertilization, EC: endothelial cell, l-CaDI: left caudal division of internal carotid artery, r-CaDI: right caudal division of internal carotid artery, BCA: basal communicating artery, l-PCS: left posterior communicating segment, r-PCS: right posterior communicating segment

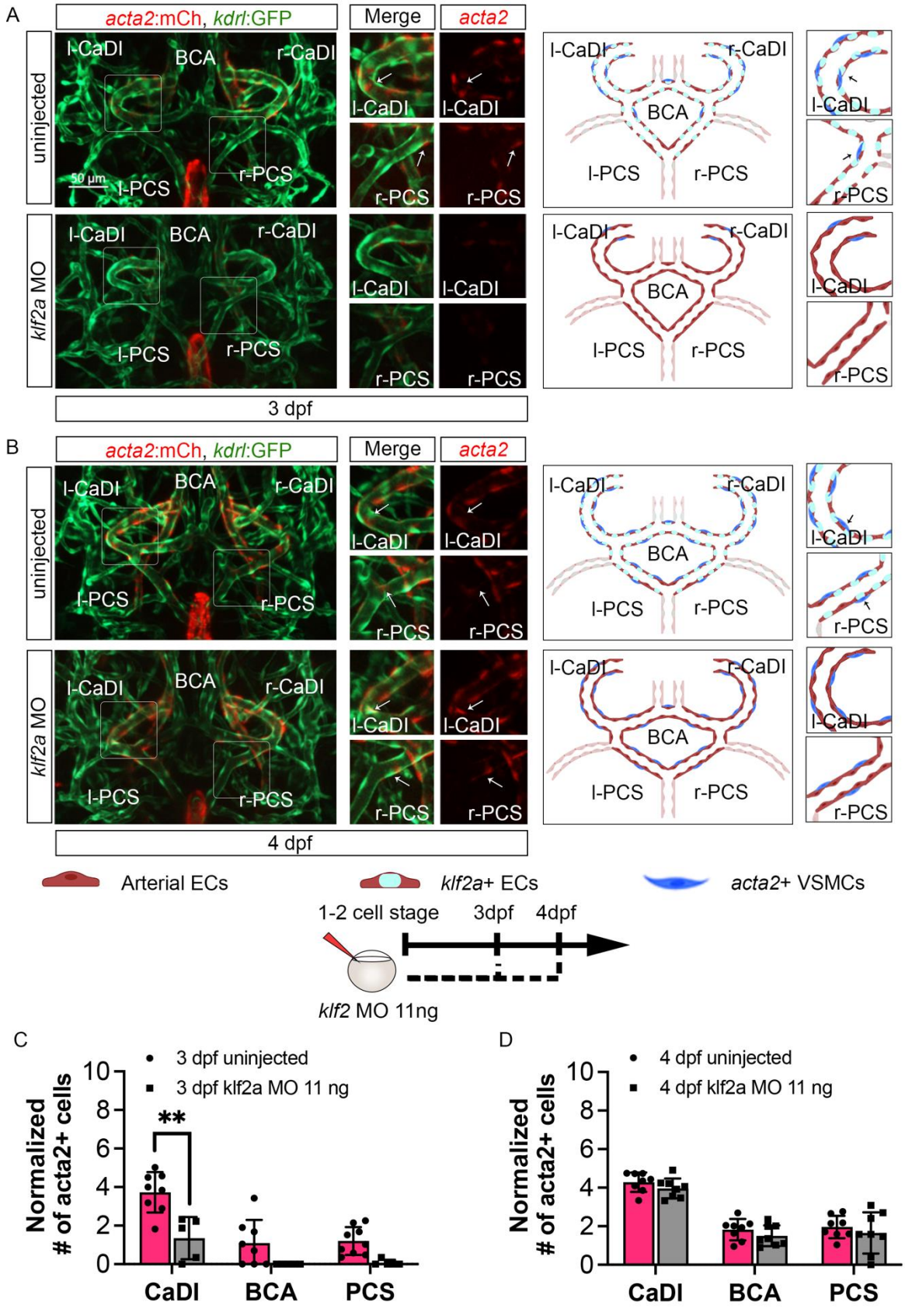

Figure 6. *klf2a* promotes vascular smooth muscle cell (VSMC) differentiation on anterior circle of Willis (CW) arteries

(A-B) Confocal live images of Tg(*acta2:mcherry*; *kdrl:gfp*)$^{ca8/zn1}$ and scheme representation of vascular endothelium and VSMCs on CW arteries at 3 dpf (A) and 4 dpf (B) in uninjected control embryos, embryos injected with 11 ng *klf2a* morpholino (MO). Red channel represents *acta2:mcherry*, Green channel represents *kdrl:gfp*, and Merge panel combines both channels. Arrows point to the CW arteries with *acta2:mcherry* signal. Scale bar = 50 µm

(C) Number of *acta2*+ VSMCs per 100 µm vessel length on caudal division of internal carotid arteries (CaDI), basal communicating artery (BCA), and posterior communicating segments (PCS) at 3 dpf in uninjected control (n=8, 2 independent experiments) and embryos injected with 11 ng *klf2a* MO at one to two cell stage (n=8, 2 independent experiments), two-tailed Mann–Whitney test on each vessel's comparison, represented with mean ± SD, ** p≤0.01

(D) Number of *acta2*+ VSMCs per 100 µm vessel length on CaDI, BCA, and PCS at 4 dpf in uninjected control (n=8, 3 independent experiments) and embryos injected with 11 ng *klf2a* MO at one to two cell stage (n=8, 3 independent experiments), two-tailed Mann–Whitney test on each vessel's comparison, represented with mean ± SD

Abbreviations: hpf: hour post fertilization, dpf: day post fertilization, EC: endothelial cell, l-CaDI: left caudal division of internal carotid artery, r-CaDI: right caudal division of internal carotid artery, BCA: basal communicating artery, l-PCS: left posterior communicating segment, r-PCS: right posterior communicating segment

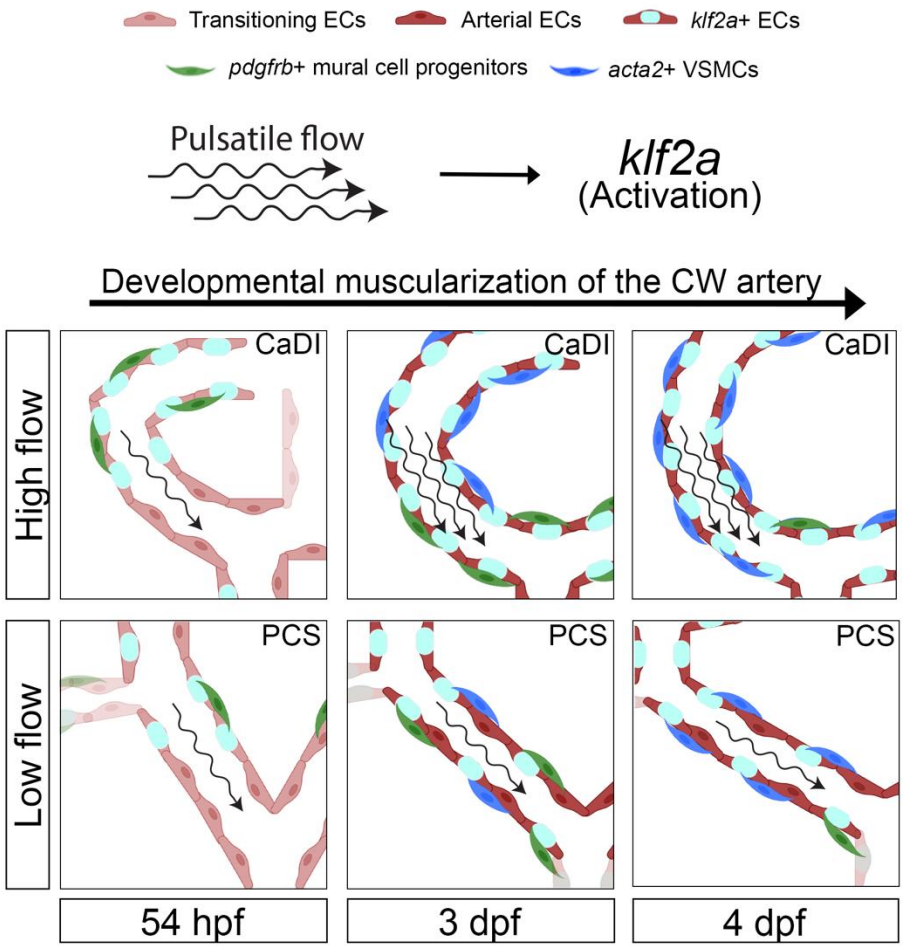

662 **Figure 7.** Schematic model of the developmental muscularization of the CW arteries

663 The model shows how pulsatile flow generate higher hemodynamics in anterior CW
664 arteries like the caudal division of internal carotid artery (CaDI) via the activation of
665 endothelial *klf2a* signaling. Other posterior CW arteries with straight shape like the
666 posterior communicating segment (PCS) experience less hemodynamic force and
667 showed moderate *klf2a* activation and VSMC differentiation.

668 Abbreviations: hpf: hour post fertilization, dpf: day post fertilization, EC: endothelial cell,
669 VSMC: vascular smooth muscle cell, CaDI: caudal division of internal carotid artery,
670 PCS: posterior communicating segment

671

672 **Supplementary Figures and Supplementary Figure Legends**

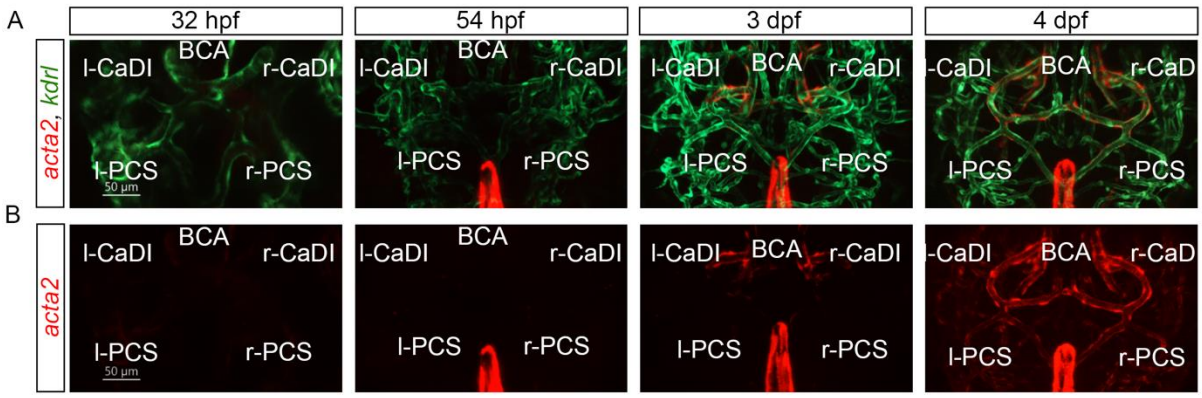

674 **Figure S1.** Vascular smooth muscle cell (VSMC) differentiation on circle of Willis (CW)
675 arteries

676 (A-B) Confocal live images of Tg(*acta2:mcherry*, *kdrl:gfp*)$^{ca8/zn1}$ in CW arteries of
677 zebrafish brain at 32 hour post fertilization (hpf), 54 hpf, 3 day post fertilization (dpf),
678 and 4 dpf. Red channel represents *acta2:mcherry*, Green channel represents *kdrl:gfp*,
679 and Merge panel combines both channels. Scale bar = 50 μm

680 Abbreviations: hpf: hour post fertilization, dpf: day post fertilization, VSMC: vascular
681 smooth muscle cell, l-CaDI: left caudal division of internal carotid artery, r-CaDI: right
682 caudal division of internal carotid artery, BCA: basal communicating artery, l-PCS: left
683 posterior communicating segment, r-PCS: right posterior communicating segment

684

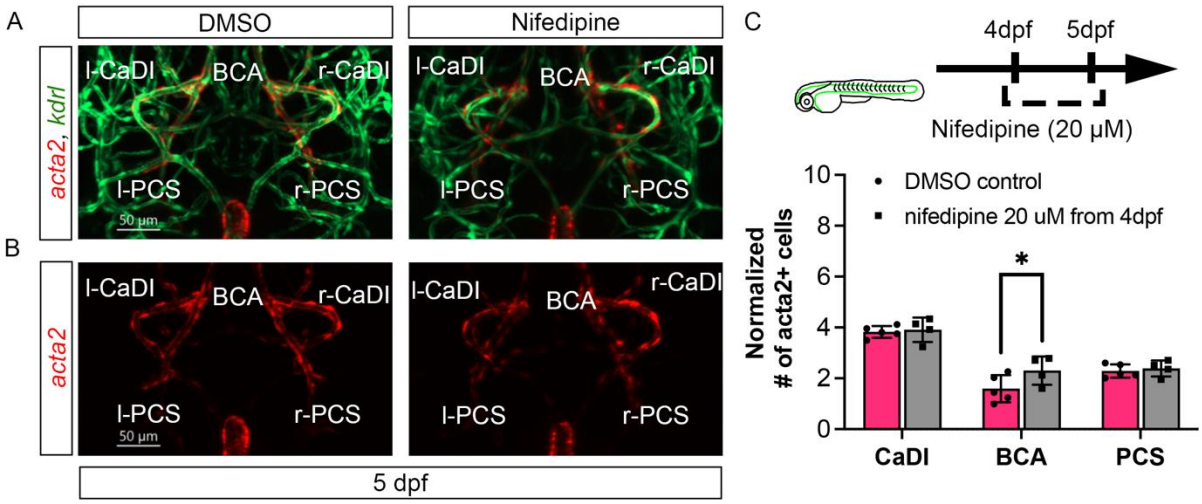

686 **Figure S2.** Blood flow is not required for vascular smooth muscle cell (VSMC)
687 maintenance on circle of Willis (CW) arteries

688 (A-B) Confocal live images of Tg(*acta2:mcherry*; *kdrl:gfp*)$^{ca8/zn1}$ in CW arteries of
689 zebrafish brain at 5 day post fertilization (dpf) in DMSO control embryos and embryos
690 treated with 20 μM nifedipine from 4 dpf. Red channel represents *acta2:mcherry*, Green
691 channel represents *kdrl:gfp*, and Merge panel combines both channels. Scale bar = 50
692 μm

693 (C) Number of *acta2*+ VSMCs per 100 μm vessel length on caudal division of internal
694 carotid arteries (CaDI), basal communicating artery (BCA), and posterior
695 communicating segments (PCS) at 5 dpf in DMSO control (n=5, 1 independent
696 experiment) and embryos treated with 20 μM nifedipine from 4 dpf (n=4, 1 independent
697 experiment), two-tailed Mann–Whitney test on each vessel's comparison, represented
698 with mean ± SD, * p≤0.05

699 Abbreviations: hpf: hour post fertilization, dpf: day post fertilization, VSMC: vascular
700 smooth muscle cell, l-CaDI: left caudal division of internal carotid artery, r-CaDI: right
701 caudal division of internal carotid artery, BCA: basal communicating artery, l-PCS: left
702 posterior communicating segment, r-PCS: right posterior communicating segment

703

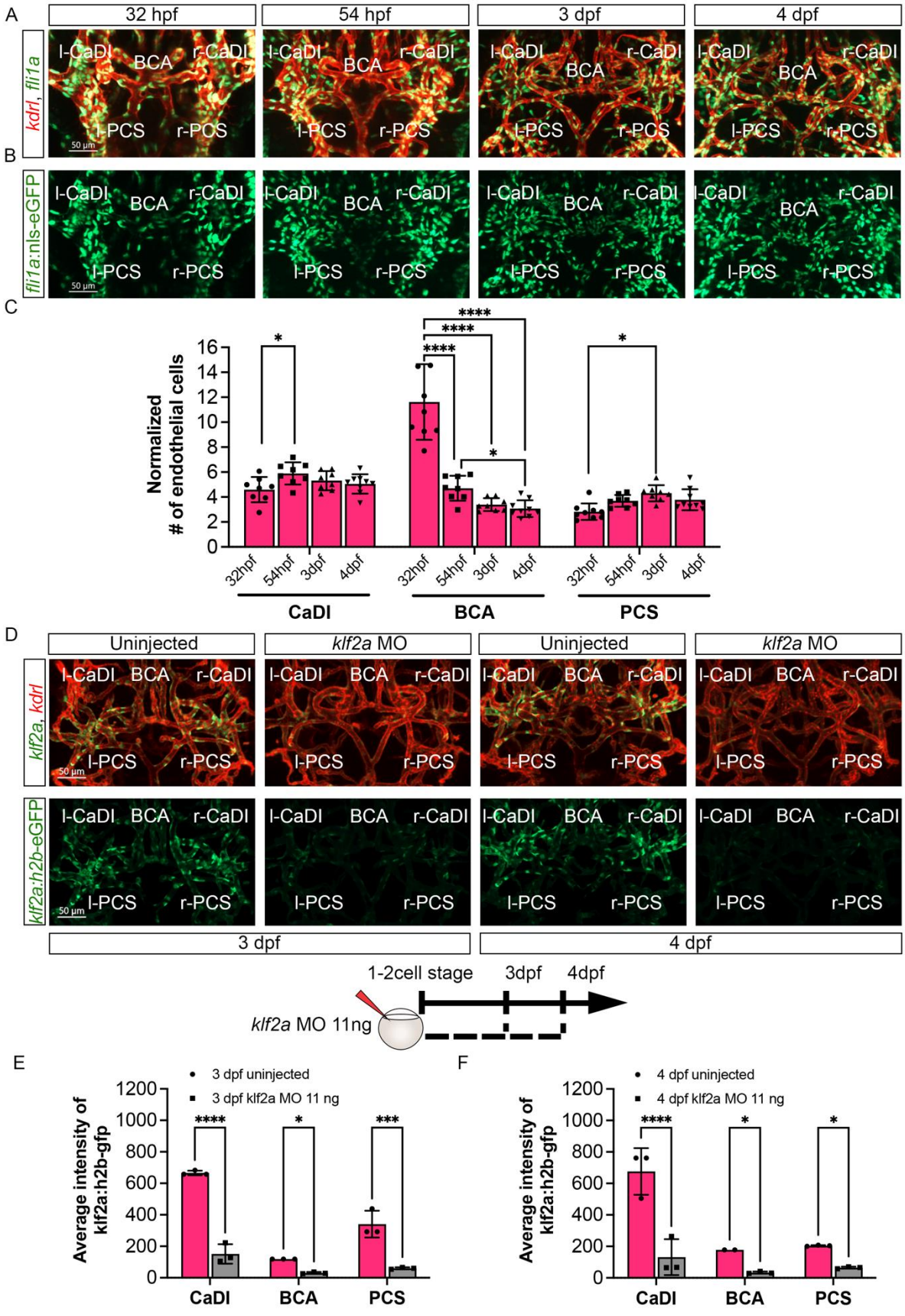

Figure S3. Number of endothelial cells (ECs) in circle of Willis (CW) arteries does not increase during *klf2a* activation

(A-B) Confocal live images of Tg(*fli1:nls-gfp*, *kdrl:ras-mcherry*)$^{y7/s896}$ in CW arteries of zebrafish brain at 32 hour post fertilization (hpf), 54 hpf, 3 day post fertilization (dpf), and 4 dpf. Red channel represents *kdrl:ras-mcherry* and Green channel represents *fli1:nls-gfp*. Scale bar = 50 μm

(C) Number of ECs per 100 μm vessel length on caudal division of internal carotid arteries (CaDI), basal communicating artery (BCA), and posterior communicating segments (PCS) at 32 hpf (n=9, 1 independent experiment), 54 hpf (n=8, 1 independent experiment), 3 dpf (n=8, 1 independent experiment), and 4 dpf (n=9, 1 independent experiment), two-way analyses of variance followed by Tukey's multiple comparisons, represented with mean ± SD, * p≤0.05, **** p≤0.0001

(D) Confocal live images of Tg(*klf2a:h2b-gfp*, *kdrl:ras-mcherry*)$^{ig11/s896}$ in CW arteries of zebrafish brain at 3 and 4 dpf in uninjected control and embryos injected with 11 ng of *klf2a* morpholino (MO). Red channel represents *kdrl:ras-mcherry* and Green channel represents *klf2a:h2b-gfp*. Scale bar = 50 μm

(E) Average intensity of *klf2a:h2b-gfp* in CaDI, BCA, and PCS at 3 dpf in uninjected control (n=3, 1 independent experiment) and embryos injected with 11 ng of *klf2a* MO (n=3, 1 independent experiment), two-tailed Mann–Whitney test on each vessel's comparison, represented with mean ± SD, * p≤0.05, *** p≤0.001, **** p≤0.0001

(F) Average intensity of *klf2a:h2b-gfp* in CaDI, BCA, and PCS at 4 dpf in uninjected control (n=3, 1 independent experiment) and embryos injected with 11 ng of *klf2a* MO (n=3, 1 independent experiment), two-tailed Mann–Whitney test on each vessel's comparison, represented with mean ± SD, * p≤0.05, **** p≤0.0001

Abbreviations: hpf: hour post fertilization, dpf: day post fertilization, l-CaDI: left caudal division of internal carotid artery, r-CaDI: right caudal division of internal carotid artery, BCA: basal communicating artery, l-PCS: left posterior communicating segment, r-PCS: right posterior communicating segment

Reference

Abello, J., Raghavan, S., Yien, Y. Y., & Stratman, A. N. (2022). Peristaltic pumps adapted for laminar flow experiments enhance in vitro modeling of vascular cell behavior. *J Biol Chem, 298*(10), 102404. doi:10.1016/j.jbc.2022.102404

Aguilar-Pineda, J. A., Vera-Lopez, K. J., Shrivastava, P., Chavez-Fumagalli, M. A., Nieto-Montesinos, R., Alvarez-Fernandez, K. L., . . . Lino Cardenas, C. L. (2021). Vascular smooth muscle cell dysfunction contribute to neuroinflammation and Tau hyperphosphorylation in Alzheimer disease. *iScience, 24*(9), 102993. doi:10.1016/j.isci.2021.102993

Ando, K., Fukuhara, S., Izumi, N., Nakajima, H., Fukui, H., Kelsh, R. N., & Mochizuki, N. (2016). Clarification of mural cell coverage of vascular endothelial cells by live imaging of zebrafish. *Development, 143*(8), 1328-1339. doi:10.1242/dev.132654

Ando, K., Shih, Y. H., Ebarasi, L., Grosse, A., Portman, D., Chiba, A., . . . Lawson, N. D. (2021). Conserved and context-dependent roles for pdgfrb signaling during zebrafish vascular mural cell development. *Dev Biol, 479*, 11-22. doi:10.1016/j.ydbio.2021.06.010

Ando, K., Tong, L., Peng, D., Vazquez-Liebanas, E., Chiyoda, H., He, L., . . . Betsholtz, C. (2022). KCNJ8/ABCC9-containing K-ATP channel modulates brain vascular smooth muscle development and neurovascular coupling. *Dev Cell, 57*(11), 1383-1399 e1387. doi:10.1016/j.devcel.2022.04.019

Ando, K., Wang, W., Peng, D., Chiba, A., Lagendijk, A. K., Barske, L., . . . Betsholtz, C. (2019). Peri-arterial specification of vascular mural cells from naive mesenchyme requires Notch signaling. *Development, 146*(2). doi:10.1242/dev.165589

ANSYS. (2014). ANSYS Innovation Courses: 3D bifurcating artery. Retrieved from https://courses.ansys.com/index.php/courses/fluent-3d-bifurcating-artery/

Bahrami, N., & Childs, S. J. (2020). Development of vascular regulation in the zebrafish embryo. *Development, 147*(10). doi:10.1242/dev.183061

Barak, T., Ristori, E., Ercan-Sencicek, A. G., Miyagishima, D. F., Nelson-Williams, C., Dong, W., . . . Gunel, M. (2021). PPIL4 is essential for brain angiogenesis and implicated in intracranial aneurysms in humans. *Nat Med, 27*(12), 2165-2175. doi:10.1038/s41591-021-01572-7

Basatemur, G. L., Jorgensen, H. F., Clarke, M. C. H., Bennett, M. R., & Mallat, Z. (2019). Vascular smooth muscle cells in atherosclerosis. *Nat Rev Cardiol, 16*(12), 727-744. doi:10.1038/s41569-019-0227-9

Biswas, S., Shahriar, S., Giangreco, N. P., Arvanitis, P., Winkler, M., Tatonetti, N. P., . . . Agalliu, D. (2022). Mural Wnt/beta-catenin signaling regulates Lama2 expression to promote neurovascular unit maturation. *Development, 149*(17). doi:10.1242/dev.200610

Boettger, T., Beetz, N., Kostin, S., Schneider, J., Kruger, M., Hein, L., & Braun, T. (2009). Acquisition of the contractile phenotype by murine arterial smooth muscle cells depends on the Mir143/145 gene cluster. *J Clin Invest, 119*(9), 2634-2647. doi:10.1172/JCI38864

Bondjers, C., He, L., Takemoto, M., Norlin, J., Asker, N., Hellstrom, M., . . . Betsholtz, C. (2006). Microarray analysis of blood microvessels from PDGF-B and PDGF-Rbeta mutant mice identifies novel markers for brain pericytes. *FASEB J, 20*(10), 1703-1705. doi:10.1096/fj.05-4944fje

776 Campbell, B. C. V., De Silva, D. A., Macleod, M. R., Coutts, S. B., Schwamm, L. H., Davis, S. M., &
777 Donnan, G. A. (2019). Ischaemic stroke. *Nat Rev Dis Primers, 5*(1), 70.
778 doi:10.1038/s41572-019-0118-8
779 Chang, L., Noseda, M., Higginson, M., Ly, M., Patenaude, A., Fuller, M., . . . Karsan, A. (2012).
780 Differentiation of vascular smooth muscle cells from local precursors during embryonic
781 and adult arteriogenesis requires Notch signaling. *Proc Natl Acad Sci U S A, 109*(18),
782 6993-6998. doi:10.1073/pnas.1118512109
783 Chasseigneaux, S., Moraca, Y., Cochois-Guegan, V., Boulay, A. C., Gilbert, A., Le Crom, S., . . .
784 Saubamea, B. (2018). Isolation and differential transcriptome of vascular smooth muscle
785 cells and mid-capillary pericytes from the rat brain. *Sci Rep, 8*(1), 12272.
786 doi:10.1038/s41598-018-30739-5
787 Chen, X., Gays, D., Milia, C., & Santoro, M. M. (2017). Cilia Control Vascular Mural Cell
788 Recruitment in Vertebrates. *Cell Rep, 18*(4), 1033-1047.
789 doi:10.1016/j.celrep.2016.12.044
790 Chen, Z., Qin, H., Liu, J., Wu, B., Cheng, Z., Jiang, Y., . . . Wang, Y. (2019). Characteristics of Wall
791 Shear Stress and Pressure of Intracranial Atherosclerosis Analyzed by a Computational
792 Fluid Dynamics Model: A Pilot Study. *Front Neurol, 10*, 1372.
793 doi:10.3389/fneur.2019.01372
794 Chi, N. C., Shaw, R. M., De Val, S., Kang, G., Jan, L. Y., Black, B. L., & Stainier, D. Y. (2008). Foxn4
795 directly regulates tbx2b expression and atrioventricular canal formation. *Genes Dev,*
796 *22*(6), 734-739. doi:10.1101/gad.1629408
797 Chou, E. L., Lino Cardenas, C. L., Chaffin, M., Arduini, A. D., Juric, D., Stone, J. R., . . . Lindsay, M.
798 E. (2022). Vascular smooth muscle cell phenotype switching in carotid atherosclerosis.
799 *JVS Vasc Sci, 3*, 41-47. doi:10.1016/j.jvssci.2021.11.002
800 Colijn, S., Nambara, M., & Stratman, A. N. (2023). Identification of overlapping and distinct
801 mural cell populations during early embryonic development. *bioRxiv*,
802 2023.2004.2003.535476. doi:10.1101/2023.04.03.535476
803 Crouch, E. E., Bhaduri, A., Andrews, M. G., Cebrian-Silla, A., Diafos, L. N., Birrueta, J. O., . . .
804 Huang, E. J. (2022). Ensembles of endothelial and mural cells promote angiogenesis in
805 prenatal human brain. *Cell, 185*(20), 3753-3769 e3718. doi:10.1016/j.cell.2022.09.004
806 Crouch, E. E., Joseph, T., Marsan, E., & Huang, E. J. (2023). Disentangling brain vasculature in
807 neurogenesis and neurodegeneration using single-cell transcriptomics. *Trends Neurosci,*
808 *46*(7), 551-565. doi:10.1016/j.tins.2023.04.007
809 Daneman, R., Agalliu, D., Zhou, L., Kuhnert, F., Kuo, C. J., & Barres, B. A. (2009). Wnt/beta-
810 catenin signaling is required for CNS, but not non-CNS, angiogenesis. *Proc Natl Acad Sci*
811 *U S A, 106*(2), 641-646. doi:10.1073/pnas.0805165106
812 Dekker, R. J., van Soest, S., Fontijn, R. D., Salamanca, S., de Groot, P. G., VanBavel, E., . . .
813 Horrevoets, A. J. (2002). Prolonged fluid shear stress induces a distinct set of endothelial
814 cell genes, most specifically lung Kruppel-like factor (KLF2). *Blood, 100*(5), 1689-1698.
815 doi:10.1182/blood-2002-01-0046
816 Domenga, V., Fardoux, P., Lacombe, P., Monet, M., Maciazek, J., Krebs, L. T., . . . Joutel, A.
817 (2004). Notch3 is required for arterial identity and maturation of vascular smooth
818 muscle cells. *Genes Dev, 18*(22), 2730-2735. doi:10.1101/gad.308904

819 Donadon, M., & Santoro, M. M. (2021). The origin and mechanisms of smooth muscle cell
820 development in vertebrates. *Development, 148*(7). doi:ARTN dev197384

821 10.1242/dev.197384
822 Duchemin, A. L., Vignes, H., & Vermot, J. (2019). Mechanically activated piezo channels
823 modulate outflow tract valve development through the Yap1 and Klf2-Notch signaling
824 axis. *Elife, 8*. doi:10.7554/eLife.44706
825 Fernandes, M. C., Sousa, L. C., de Castro, C. F., da Palma, J. M. L. M., António, C. C., & Pinto, S. I.
826 S. (2022). Implementation and Comparison of Non-Newtonian Viscosity Models in
827 Hemodynamic Simulations of Patient Coronary Arteries. In *Theoretical Analyses,*
828 *Computations, and Experiments of Multiscale Materials: A Tribute to Francesco dell'Isola*
829 (pp. 403-428): Springer.
830 Fontana, F., Haack, T., Reichenbach, M., Knaus, P., Puceat, M., & Abdelilah-Seyfried, S. (2020).
831 Antagonistic Activities of Vegfr3/Flt4 and Notch1b Fine-tune Mechanosensitive Signaling
832 during Zebrafish Cardiac Valvulogenesis. *Cell Rep, 32*(2), 107883.
833 doi:10.1016/j.celrep.2020.107883
834 Fox, B. M., Dorschel, K. B., Lawton, M. T., & Wanebo, J. E. (2021). Pathophysiology of Vascular
835 Stenosis and Remodeling in Moyamoya Disease. *Front Neurol, 12*, 661578.
836 doi:10.3389/fneur.2021.661578
837 Franco, C. A., Jones, M. L., Bernabeu, M. O., Vion, A. C., Barbacena, P., Fan, J., . . . Gerhardt, H.
838 (2016). Non-canonical Wnt signalling modulates the endothelial shear stress flow sensor
839 in vascular remodelling. *Elife, 5*, e07727. doi:10.7554/eLife.07727
840 Fujita, M., Cha, Y. R., Pham, V. N., Sakurai, A., Roman, B. L., Gutkind, J. S., & Weinstein, B. M.
841 (2011). Assembly and patterning of the vascular network of the vertebrate hindbrain.
842 *Development, 138*(9), 1705-1715. doi:10.1242/dev.058776
843 Gierten, J., Pylatiuk, C., Hammouda, O. T., Schock, C., Stegmaier, J., Wittbrodt, J., . . . Loosli, F.
844 (2020). Automated high-throughput heartbeat quantification in medaka and zebrafish
845 embryos under physiological conditions. *Sci Rep, 10*(1), 2046. doi:10.1038/s41598-020-
846 58563-w
847 Goddard, L. M., Duchemin, A. L., Ramalingan, H., Wu, B., Chen, M., Bamezai, S., . . . Kahn, M. L.
848 (2017). Hemodynamic Forces Sculpt Developing Heart Valves through a KLF2-WNT9B
849 Paracrine Signaling Axis. *Dev Cell, 43*(3), 274-289 e275.
850 doi:10.1016/j.devcel.2017.09.023
851 Gray, K. M., & Stroka, K. M. (2017). Vascular endothelial cell mechanosensing: New insights
852 gained from biomimetic microfluidic models. *Semin Cell Dev Biol, 71*, 106-117.
853 doi:10.1016/j.semcdb.2017.06.002
854 Griffith, C. M., Huang, S. A., Cho, C., Khare, T. M., Rich, M., Lee, G. H., . . . Polacheck, W. J.
855 (2020). Microfluidics for the study of mechanotransduction. *J Phys D Appl Phys, 53*(22).
856 doi:10.1088/1361-6463/ab78d4
857 Guo, D. C., Pannu, H., Tran-Fadulu, V., Papke, C. L., Yu, R. K., Avidan, N., . . . Milewicz, D. M.
858 (2007). Mutations in smooth muscle alpha-actin (ACTA2) lead to thoracic aortic
859 aneurysms and dissections. *Nat Genet, 39*(12), 1488-1493. doi:10.1038/ng.2007.6
860 Guo, D. C., Papke, C. L., Tran-Fadulu, V., Regalado, E. S., Avidan, N., Johnson, R. J., . . . Milewicz,
861 D. M. (2009). Mutations in smooth muscle alpha-actin (ACTA2) cause coronary artery

disease, stroke, and Moyamoya disease, along with thoracic aortic disease. *Am J Hum Genet, 84*(5), 617-627. doi:10.1016/j.ajhg.2009.04.007

Hasan, S. S., Tsaryk, R., Lange, M., Wisniewski, L., Moore, J. C., Lawson, N. D., . . . Siekmann, A. F. (2017). Endothelial Notch signalling limits angiogenesis via control of artery formation. *Nat Cell Biol, 19*(8), 928-940. doi:10.1038/ncb3574

He, L., Vanlandewijck, M., Raschperger, E., Andaloussi Mae, M., Jung, B., Lebouvier, T., . . . Betsholtz, C. (2016). Analysis of the brain mural cell transcriptome. *Sci Rep, 6*, 35108. doi:10.1038/srep35108

Hergenreider, E., Heydt, S., Treguer, K., Boettger, T., Horrevoets, A. J., Zeiher, A. M., . . . Dimmeler, S. (2012). Atheroprotective communication between endothelial cells and smooth muscle cells through miRNAs. *Nat Cell Biol, 14*(3), 249-256. doi:10.1038/ncb2441

High, F. A., Lu, M. M., Pear, W. S., Loomes, K. M., Kaestner, K. H., & Epstein, J. A. (2008). Endothelial expression of the Notch ligand Jagged1 is required for vascular smooth muscle development. *Proc Natl Acad Sci U S A, 105*(6), 1955-1959. doi:10.1073/pnas.0709663105

Hill, R. A., Tong, L., Yuan, P., Murikinati, S., Gupta, S., & Grutzendler, J. (2015). Regional Blood Flow in the Normal and Ischemic Brain Is Controlled by Arteriolar Smooth Muscle Cell Contractility and Not by Capillary Pericytes. *Neuron, 87*(1), 95-110. doi:10.1016/j.neuron.2015.06.001

Hogan, B. M., Herpers, R., Witte, M., Helotera, H., Alitalo, K., Duckers, H. J., & Schulte-Merker, S. (2009). Vegfc/Flt4 signalling is suppressed by Dll4 in developing zebrafish intersegmental arteries. *Development, 136*(23), 4001-4009. doi:10.1242/dev.039990

Huang, J., Cheng, L., Li, J., Chen, M., Zhou, D., Lu, M. M., . . . Parmacek, M. S. (2008). Myocardin regulates expression of contractile genes in smooth muscle cells and is required for closure of the ductus arteriosus in mice. *J Clin Invest, 118*(2), 515-525. doi:10.1172/JCI33304

Humphrey, J. D., & Schwartz, M. A. (2021). Vascular Mechanobiology: Homeostasis, Adaptation, and Disease. *Annu Rev Biomed Eng, 23*, 1-27. doi:10.1146/annurev-bioeng-092419-060810

Isogai, S., Horiguchi, M., & Weinstein, B. M. (2001). The vascular anatomy of the developing zebrafish: an atlas of embryonic and early larval development. *Dev Biol, 230*(2), 278-301. doi:10.1006/dbio.2000.9995

Joutel, A., Corpechot, C., Ducros, A., Vahedi, K., Chabriat, H., Mouton, P., . . . Tournier-Lasserve, E. (1996). Notch3 mutations in CADASIL, a hereditary adult-onset condition causing stroke and dementia. *Nature, 383*(6602), 707-710. doi:10.1038/383707a0

Kaplan, L., Chow, B. W., & Gu, C. (2020). Neuronal regulation of the blood-brain barrier and neurovascular coupling. *Nat Rev Neurosci, 21*(8), 416-432. doi:10.1038/s41583-020-0322-2

Katritsis, D., Kaiktsis, L., Chaniotis, A., Pantos, J., Efstathopoulos, E. P., & Marmarelis, V. (2007). Wall shear stress: theoretical considerations and methods of measurement. *Prog Cardiovasc Dis, 49*(5), 307-329. doi:10.1016/j.pcad.2006.11.001

Lawson, N. D., Scheer, N., Pham, V. N., Kim, C. H., Chitnis, A. B., Campos-Ortega, J. A., & Weinstein, B. M. (2001). Notch signaling is required for arterial-venous differentiation

during embryonic vascular development. *Development, 128*(19), 3675-3683. doi:10.1242/dev.128.19.3675

Lee, J. S., Yu, Q., Shin, J. T., Sebzda, E., Bertozzi, C., Chen, M., . . . Kahn, M. L. (2006). Klf2 is an essential regulator of vascular hemodynamic forces in vivo. *Dev Cell, 11*(6), 845-857. doi:10.1016/j.devcel.2006.09.006

Li, S., Wang, D. Z., Wang, Z., Richardson, J. A., & Olson, E. N. (2003). The serum response factor coactivator myocardin is required for vascular smooth muscle development. *Proc Natl Acad Sci U S A, 100*(16), 9366-9370. doi:10.1073/pnas.1233635100

Liebner, S., Corada, M., Bangsow, T., Babbage, J., Taddei, A., Czupalla, C. J., . . . Dejana, E. (2008). Wnt/beta-catenin signaling controls development of the blood-brain barrier. *J Cell Biol, 183*(3), 409-417. doi:10.1083/jcb.200806024

Lin, R., Xie, Z., Zhang, J., Xu, H., Su, H., Tan, X., . . . Su, M. (2012). Clinical and immunopathological features of Moyamoya disease. *PLoS One, 7*(4), e36386. doi:10.1371/journal.pone.0036386

Mack, C. P., & Owens, G. K. (1999). Regulation of smooth muscle alpha-actin expression in vivo is dependent on CArG elements within the 5' and first intron promoter regions. *Circ Res, 84*(7), 852-861. doi:10.1161/01.res.84.7.852

Mack, J. J., Mosqueiro, T. S., Archer, B. J., Jones, W. M., Sunshine, H., Faas, G. C., . . . Iruela-Arispe, M. L. (2017). NOTCH1 is a mechanosensor in adult arteries. *Nat Commun, 8*(1), 1620. doi:10.1038/s41467-017-01741-8

Milewicz, D. M., Kwartler, C. S., Papke, C. L., Regalado, E. S., Cao, J., & Reid, A. J. (2010). Genetic variants promoting smooth muscle cell proliferation can result in diffuse and diverse vascular diseases: evidence for a hyperplastic vasculomyopathy. *Genet Med, 12*(4), 196-203. doi:10.1097/GIM.0b013e3181cdd687

Mill, C., & George, S. J. (2012). Wnt signalling in smooth muscle cells and its role in cardiovascular disorders. *Cardiovasc Res, 95*(2), 233-240. doi:10.1093/cvr/cvs141

Mirabella, T., MacArthur, J. W., Cheng, D., Ozaki, C. K., Woo, Y. J., Yang, M., & Chen, C. S. (2017). 3D-printed vascular networks direct therapeutic angiogenesis in ischaemia. *Nat Biomed Eng, 1*. doi:10.1038/s41551-017-0083

Nicoli, S., Standley, C., Walker, P., Hurlstone, A., Fogarty, K. E., & Lawson, N. D. (2010). MicroRNA-mediated integration of haemodynamics and Vegf signalling during angiogenesis. *Nature, 464*(7292), 1196-1200. doi:10.1038/nature08889

Oka, M., Shimo, S., Ohno, N., Imai, H., Abekura, Y., Koseki, H., . . . Aoki, T. (2020). Dedifferentiation of smooth muscle cells in intracranial aneurysms and its potential contribution to the pathogenesis. *Sci Rep, 10*(1), 8330. doi:10.1038/s41598-020-65361-x

Page, D. M., Wittamer, V., Bertrand, J. Y., Lewis, K. L., Pratt, D. N., Delgado, N., . . . Traver, D. (2013). An evolutionarily conserved program of B-cell development and activation in zebrafish. *Blood, 122*(8), e1-11. doi:10.1182/blood-2012-12-471029

Paolini, A., Fontana, F., Pham, V. C., Rodel, C. J., & Abdelilah-Seyfried, S. (2021). Mechanosensitive Notch-Dll4 and Klf2-Wnt9 signaling pathways intersect in guiding valvulogenesis in zebrafish. *Cell Rep, 37*(1), 109782. doi:10.1016/j.celrep.2021.109782

Parmar, K. M., Larman, H. B., Dai, G., Zhang, Y., Wang, E. T., Moorthy, S. N., . . . Garcia-Cardena, G. (2006). Integration of flow-dependent endothelial phenotypes by Kruppel-like factor 2. *J Clin Invest, 116*(1), 49-58. doi:10.1172/JCI24787

Pitulescu, M. E., Schmidt, I., Giaimo, B. D., Antoine, T., Berkenfeld, F., Ferrante, F., . . . Adams, R. H. (2017). Dll4 and Notch signalling couples sprouting angiogenesis and artery formation. *Nat Cell Biol, 19*(8), 915-927. doi:10.1038/ncb3555

Polacheck, W. J., Kutys, M. L., Yang, J., Eyckmans, J., Wu, Y., Vasavada, H., . . . Chen, C. S. (2017). A non-canonical Notch complex regulates adherens junctions and vascular barrier function. *Nature, 552*(7684), 258-262. doi:10.1038/nature24998

Robin, Y. M., Penel, N., Perot, G., Neuville, A., Velasco, V., Ranchere-Vince, D., . . . Coindre, J. M. (2013). Transgelin is a novel marker of smooth muscle differentiation that improves diagnostic accuracy of leiomyosarcomas: a comparative immunohistochemical reappraisal of myogenic markers in 900 soft tissue tumors. *Mod Pathol, 26*(4), 502-510. doi:10.1038/modpathol.2012.192

Roman, B. L., Pham, V. N., Lawson, N. D., Kulik, M., Childs, S., Lekven, A. C., . . . Weinstein, B. M. (2002). Disruption of acvrl1 increases endothelial cell number in zebrafish cranial vessels. *Development, 129*(12), 3009-3019. doi:10.1242/dev.129.12.3009

Schröder, H., Moser, N., & Huggenberger, S. (2020). The Mouse Circle of Willis. In *Neuroanatomy of the Mouse: An Introduction* (pp. 333-340). Cham: Springer International Publishing.

Sehnert, A. J., Huq, A., Weinstein, B. M., Walker, C., Fishman, M., & Stainier, D. Y. (2002). Cardiac troponin T is essential in sarcomere assembly and cardiac contractility. *Nat Genet, 31*(1), 106-110. doi:10.1038/ng875

Shutter, J. R., Scully, S., Fan, W., Richards, W. G., Kitajewski, J., Deblandre, G. A., . . . Stark, K. L. (2000). Dll4, a novel Notch ligand expressed in arterial endothelium. *Genes Dev, 14*(11), 1313-1318. Retrieved from https://www.ncbi.nlm.nih.gov/pubmed/10837024

Steed, E., Faggianelli, N., Roth, S., Ramspacher, C., Concordet, J. P., & Vermot, J. (2016). klf2a couples mechanotransduction and zebrafish valve morphogenesis through fibronectin synthesis. *Nat Commun, 7*, 11646. doi:10.1038/ncomms11646

Stratman, A. N., Burns, M. C., Farrelly, O. M., Davis, A. E., Li, W., Pham, V. N., . . . Weinstein, B. M. (2020). Chemokine mediated signalling within arteries promotes vascular smooth muscle cell recruitment. *Commun Biol, 3*(1), 734. doi:10.1038/s42003-020-01462-7

Stratman, A. N., Pezoa, S. A., Farrelly, O. M., Castranova, D., Dye, L. E., 3rd, Butler, M. G., . . . Weinstein, B. M. (2017). Interactions between mural cells and endothelial cells stabilize the developing zebrafish dorsal aorta. *Development, 144*(1), 115-127. doi:10.1242/dev.143131

Sweet, D. R., Fan, L., Hsieh, P. N., & Jain, M. K. (2018). Kruppel-Like Factors in Vascular Inflammation: Mechanistic Insights and Therapeutic Potential. *Front Cardiovasc Med, 5*, 6. doi:10.3389/fcvm.2018.00006

Sweet, D. R., Padmanabhan, R., Liao, X., Dashora, H. R., Tang, X., Nayak, L., . . . Jain, M. K. (2023). Kruppel-Like Factors Orchestrate Endothelial Gene Expression Through Redundant and Non-Redundant Enhancer Networks. *J Am Heart Assoc, 12*(4), e024303. doi:10.1161/JAHA.121.024303

Ulrich, F., Ma, L. H., Baker, R. G., & Torres-Vazquez, J. (2011). Neurovascular development in the embryonic zebrafish hindbrain. *Dev Biol, 357*(1), 134-151. doi:10.1016/j.ydbio.2011.06.037

Vanlandewijck, M., He, L., Mae, M. A., Andrae, J., Ando, K., Del Gaudio, F., . . . Betsholtz, C. (2018). A molecular atlas of cell types and zonation in the brain vasculature. *Nature, 554*(7693), 475-480. doi:10.1038/nature25739

Vila Cuenca, M., Cochrane, A., van den Hil, F. E., de Vries, A. A. F., Lesnik Oberstein, S. A. J., Mummery, C. L., & Orlova, V. V. (2021). Engineered 3D vessel-on-chip using hiPSC-derived endothelial- and vascular smooth muscle cells. *Stem Cell Reports, 16*(9), 2159-2168. doi:10.1016/j.stemcr.2021.08.003

Villa, N., Walker, L., Lindsell, C. E., Gasson, J., Iruela-Arispe, M. L., & Weinmaster, G. (2001). Vascular expression of Notch pathway receptors and ligands is restricted to arterial vessels. *Mech Dev, 108*(1-2), 161-164. doi:10.1016/s0925-4773(01)00469-5

Volz, K. S., Jacobs, A. H., Chen, H. I., Poduri, A., McKay, A. S., Riordan, D. P., . . . Red-Horse, K. (2015). Pericytes are progenitors for coronary artery smooth muscle. *Elife, 4*. doi:10.7554/eLife.10036

Wang, Q., Zhao, N., Kennard, S., & Lilly, B. (2012). Notch2 and Notch3 function together to regulate vascular smooth muscle development. *PLoS One, 7*(5), e37365. doi:10.1371/journal.pone.0037365

Wang, Y., Pan, L., Moens, C. B., & Appel, B. (2014). Notch3 establishes brain vascular integrity by regulating pericyte number. *Development, 141*(2), 307-317. doi:10.1242/dev.096107

Warboys, C. M., Amini, N., de Luca, A., & Evans, P. C. (2011). The role of blood flow in determining the sites of atherosclerotic plaques. *F1000 Med Rep, 3*, 5. doi:10.3410/M3-5

Watterston, C., Zeng, L., Onabadejo, A., & Childs, S. J. (2019). MicroRNA26 attenuates vascular smooth muscle maturation via endothelial BMP signalling. *PLoS Genet, 15*(5), e1008163. doi:10.1371/journal.pgen.1008163

Whitesell, T. R., Chrystal, P. W., Ryu, J. R., Munsie, N., Grosse, A., French, C. R., . . . Childs, S. J. (2019). foxc1 is required for embryonic head vascular smooth muscle differentiation in zebrafish. *Dev Biol, 453*(1), 34-47. doi:10.1016/j.ydbio.2019.06.005

Whitesell, T. R., Kennedy, R. M., Carter, A. D., Rollins, E. L., Georgijevic, S., Santoro, M. M., & Childs, S. J. (2014). An alpha-smooth muscle actin (acta2/alphasma) zebrafish transgenic line marking vascular mural cells and visceral smooth muscle cells. *PLoS One, 9*(3), e90590. doi:10.1371/journal.pone.0090590

Wu, J., Bohanan, C. S., Neumann, J. C., & Lingrel, J. B. (2008). KLF2 transcription factor modulates blood vessel maturation through smooth muscle cell migration. *J Biol Chem, 283*(7), 3942-3950. doi:10.1074/jbc.M707882200

Zhong, H., Wu, X., Huang, H., Fan, Q., Zhu, Z., & Lin, S. (2006). Vertebrate MAX-1 is required for vascular patterning in zebrafish. *Proc Natl Acad Sci U S A, 103*(45), 16800-16805. doi:10.1073/pnas.0603959103

Zhou, Y., Wang, Y., Tischfield, M., Williams, J., Smallwood, P. M., Rattner, A., . . . Nathans, J. (2014). Canonical WNT signaling components in vascular development and barrier formation. *J Clin Invest, 124*(9), 3825-3846. doi:10.1172/JCI76431